Distinct release properties of glutamate/GABA co-transmission serve as a frequency-dependent filtering of supramammillary inputs

Himawari Hirai[1], Kohtarou Konno[2], Miwako Yamasaki[2], Masahiko Watanabe[2], Takeshi Sakaba[1], Yuki Hashimotodani[1*]

[1]Graduate School of Brain Science, Doshisha University, Kyoto 610-0394, Japan
[2]Department of Anatomy, Faculty of Medicine, Hokkaido University, Sapporo, Japan

*To whom correspondence should be addressed:
Yuki Hashimotodani, PhD
Graduate School of Brain Science
Doshisha University
1-3 Tatara Miyakodani, Kyotanabe, Kyoto
610-0394, Japan
Phone: +81-774-65-6057
E-mail: hashimotodani@gmail.com

Abstract

Glutamate and GABA co-transmitting neurons exist in several brain regions; however, the mechanism by which these two neurotransmitters are co-released from the same synaptic terminals remains unclear. Here, we show that the supramammillary nucleus (SuM) to dentate granule cell synapses, which co-release glutamate and GABA, exhibit differences between glutamate and GABA release properties in paired-pulse ratio, Ca^{2+}-sensitivity, presynaptic receptor modulation, and Ca^{2+} channel-vesicle coupling configuration. Moreover, uniquantal synaptic responses show independent glutamatergic and GABAergic responses. Morphological analysis reveals that most SuM terminals form distinct glutamatergic and GABAergic synapses in proximity, each characterized by GluN1 and $GABA_A\alpha1$ labeling, respectively. Notably, glutamate/GABA co-transmission exhibits distinct short-term plasticities, with frequency-dependent depression of glutamate and frequency-independent stable depression of GABA. Our findings suggest that glutamate and GABA are co-released from different synaptic vesicles within the SuM terminals, and reveal that distinct transmission modes of glutamate/GABA co-release serve as frequency-dependent filters of SuM inputs.

Introduction

Despite the classical view of Dale's Principle known as "one neuron, one transmitter" (Eccles et al., 1954), a growing body of evidence has demonstrated that many types of neurons in several brain regions co-release multiple neurotransmitters including classical neurotransmitters (glutamate, GABA, glycine, and acetylcholine), monoamines, purines, and neuropeptides (Hnasko and Edwards, 2012; Vaaga et al., 2014; Trudeau and El Mestikawy, 2018; Wallace and Sabatini, 2023). While this co-release is thought to contribute to several brain functions (Nusbaum et al., 2001; Trudeau et al., 2014; Tritsch et al., 2016; Ma et al., 2018; Kim and Sabatini, 2023), little is known about the functional implications of the co-release of two or more neurotransmitters into neural circuits and the molecular mechanisms of how multiple neurotransmitters are co-transmitted. Here, we define co-release as the release of multiple neurotransmitters from a single neuron, regardless of whether the neurotransmitters are packaged in the same or different synaptic vesicles, and co-transmission as synaptic transmission occurring by multiple neurotransmitters and detected by distinct postsynaptic receptors (Wallace and Sabatini, 2023).

The cellular and molecular mechanisms of co-release are diverse across brain areas. In particular, the transmission modes of co-release, whether two neurotransmitters are released from the same vesicles or separate vesicles, and whether they are released from the same release sites or spatially segregated release sites, depend on the cell type in a given circuit. Co-packaging of GABA/glycine or glutamate/acetylcholine is found in the spinal cord (Jonas et al., 1998) and brainstem (Nabekura et al., 2004), and in the axon terminals of the medial habenula in the interpeduncular nucleus (Ren et al., 2011; Frahm et al., 2015), respectively. In contrast, the co-release of GABA and acetylcholine from different synaptic vesicles has been reported in the retina (Lee et al., 2010), frontal cortex (Saunders et al., 2015), and hippocampus (Takacs et al., 2018). Furthermore, the spatially segregated co-release of glutamate/glycine or glutamate/dopamine has been reported in a subset of retinal amacrine cells (Lee et al., 2016), as well as in the axon terminals from a subset of midbrain dopamine neurons (Zhang et al., 2015; Fortin et al., 2019), respectively. Importantly, dual-transmitter co-release from distinct vesicle populations or release sites can result in different release properties (Lee et al., 2010; Sengupta et al., 2017; Takacs et al., 2018; Silm et al., 2019; Zych and Ford, 2022) and induce diverse effects to spatially different postsynaptic target cells (Lee et al., 2016; Sengupta et al., 2017; Granger et al., 2020). These divergent transmission properties of co-release can regulate the circuit functions underlying distinct physiological and behavioral roles.

The co-release of glutamate and GABA, both fast-acting and functionally opposing neurotransmitters, has recently been identified in several brain regions of the adult brain (Trudeau and El Mestikawy, 2018; Kim and Sabatini, 2023; Wallace and Sabatini, 2023). In particular, the lateral habenula and dentate gyrus (DG) of the hippocampus have been extensively studied for the co-release of glutamate and GABA. The lateral habenula neurons receive glutamate/GABA co-releasing synaptic inputs from the entopeduncular nucleus (EP) (Shabel et al., 2014; Wallace et al., 2017; Root et al., 2018) and ventral tegmental area (VTA) (Root et al., 2014; Yoo et al., 2016; Root et al., 2018). Hypothalamic supramammillary nucleus (SuM) neurons projecting to the DG also co-release glutamate and GABA (Pedersen et al., 2017; Hashimotodani et al., 2018; Billwiller et al., 2020; Chen et al., 2020; Li et al., 2020; Ajibola et al., 2021). To understand how synaptic inputs mediated by the co-release of the excitatory action of glutamate and the inhibitory action of GABA are integrated and impact postsynaptic cells, it is necessary to elucidate how glutamate and GABA are co-released from the synaptic terminals. Mechanistically, if glutamate and GABA are co-released from distinct vesicle populations, each release could be differently regulated by distinct release mechanisms. Such distinct co-release modes of glutamate and GABA are expected to implement different presynaptic plasticity, which will have diverse effects on postsynaptic neurons in response to different activity patterns. By contrast, if two neurotransmitters are co-released from the same synaptic vesicles, both glutamate and GABA release are expected to be under the same regulation.

Whether glutamate and GABA are packaged in the same or separate vesicles remains controversial. Electrophysiological studies have demonstrated the co-packaging of glutamate and GABA in the same synaptic vesicles at EP-lateral habenular synapses (Shabel et al., 2014; Kim et al., 2022). Conversely, an immunoelectron microscopy (immuno-EM) study demonstrated that glutamatergic and GABAergic vesicle populations are segregated in the axon terminals of the EP and VTA projections in the lateral habenula, and that single terminals form both excitatory and inhibitory synapses (Root et al., 2018). The same study also reported that glutamate and GABA are segregated into distinct vesicle populations within the axon terminals of the SuM projections in the DG (Root et al., 2018). However, the mode of co-release of glutamate and GABA from the SuM terminals has never been functionally addressed.

In this study, we investigated the release properties of glutamate/GABA co-transmission at SuM-dentate granule cell (GC) synapses. We demonstrate that glutamate/GABA co-transmission shows independent synaptic responses and differential short-term plasticity and that their postsynaptic targets are segregated. Our results suggest that the segregation of two

115 different populations of transmitters makes it possible to exert short-term dynamic changes in
116 the co-transmission balance of glutamate and GABA and modulate GC activity in a frequency-
117 dependent manner.
118
119 **Results**
120 **Glutamate/GABA co-transmission shows different release probabilities and Ca^{2+}**
121 **sensitivities**
122 To optogenetically stimulate SuM inputs in the DG, channelrhodopsin-2 (ChR2) was expressed
123 in SuM neurons by injecting a Cre-dependent adeno-associated virus (AAV) encoding ChR2-
124 eYFP (AAV-DIO-ChR2(H134R)-eYFP) into the lateral SuM of vesicular glutamate transporter
125 2 (VGluT2)-Cre mice (Hashimotodani et al., 2018; Hirai et al., 2022; Tabuchi et al., 2022)
126 (Figures 1 A and 1B). Consistent with previous reports (Boulland et al., 2009; Soussi et al.,
127 2010; Root et al., 2018; Billwiller et al., 2020; Ajibola et al., 2021), the vast majority of ChR2-
128 eYFP-expressing SuM boutons in the DG co-expressed VGluT2 and vesicular GABA
129 transporter (vesicular inhibitory amino acid transporter, VIAAT) (Figures 1C-1E). We
130 performed whole-cell patch-clamp recordings from GCs in acute hippocampal slices and
131 recorded optically evoked excitatory or inhibitory postsynaptic currents (EPSCs or IPSCs) at
132 SuM-GC synapses in the presence of picrotoxin or NBQX/D-AP5, respectively. To examine
133 whether the co-release of glutamate and GABA exhibits the same or different release properties,
134 we first monitored the paired-pulse ratio (PPR), an index of the change in presynaptic
135 transmitter release (Zucker and Regehr, 2002), of glutamate/GABA co-transmission by paired
136 stimulation (inter-stimulus interval: 100 ms). As reported previously (Hashimotodani et al.,
137 2018; Tabuchi et al., 2022), both EPSCs and IPSCs at SuM-GC synapses exhibited paired-
138 pulse depression (Figure 1F). Importantly, we found that PPR was significantly different
139 between EPSCs and IPSCs; EPSCs were more depressed than IPSCs (Figure 1G) (EPSC: 0.46
140 $\pm$ 0.03, n = 8; IPSC: 0.6 $\pm$ 0.03, n = 8, $p < 0.01$, unpaired t test). It is possible that direct
141 illumination of presynaptic terminals could increase transmitter release due to the broadening
142 of the presynaptic waveform or direct influx of Ca^{2+} through ChR2 (Jackman et al., 2014; Rost
143 et al., 2022). To avoid this possibility, we stimulated SuM axons instead of SuM terminals
144 (Figure 1-figure supplement 1A and 1B), and obtained similar results to terminal illumination
145 (Figure 1-figure supplement 1C-F). ChR2 desensitization could depress the second synaptic
146 responses evoked by the paired-pulse stimulation due to the participation of fewer SuM fibers
147 in mediating synaptic transmission. To test this possibility, the fiber volley evoked by light
148 illumination was extracellularly recorded from supragranular layer. We found that the
149 amplitudes of the second fiber volley was comparable to that of the first fiber volley (Figure 1-
150 figure supplement 2), suggesting that ChR2-expressing SuM fibers were activated to the same
151 extent by paired-pulse light illumination. Altogether, these results suggest that the release

152 probability differs between the co-released glutamate and GABA from SuM terminals in the
153 DG.

154 Since vesicular exocytosis depends on the extracellular Ca^{2+} concentration, we next
155 examined whether reducing the release probability by lowering the extracellular Ca^{2+}
156 concentration could have different effects on glutamate/GABA co-transmission. Reducing
157 extracellular Ca^{2+} concentration from 2.5 to 1 mM decreased the amplitudes of EPSCs and
158 IPSCs (Figure 1H) (EPSC: $n = 14$, $p < 0.001$, paired t test; IPSC: $n = 15$, $p < 0.001$, paired t
159 test). Remarkably, IPSCs decreased to a greater extent than EPSCs (Figure 1I) (EPSC: 45.1 ±
160 4.1% of reduction, $n = 14$; IPSC: 58.2 ± 2.7% of reduction, $n = 15$, $p < 0.01$, unpaired t test),
161 suggesting different Ca^{2+} sensitivities for glutamate and GABA release.

162

163 **Co-release of glutamate and GABA differs in presynaptic modulation and Ca^{2+} channel-**
164 **vesicle coupling configuration**

165 To further investigate whether the release properties of glutamate and GABA at SuM-GC
166 synapses are different, we next examined whether glutamate and GABA co-release are
167 mediated by different types of Ca^{2+} channels. We found that the application of ω-conotoxin-
168 GVIA (ω-CgTx), an N-type Ca^{2+} channel blocker, had no effect on EPSCs or IPSCs at SuM-
169 GC synapses (Figure 2A) (EPSC: 92.5 ± 13.8% of baseline, $n = 6$, $p = 0.53$, Wilcoxon signed-
170 rank test; IPSC: 101.7 ± 11% of baseline, $n = 6$, $p = 0.89$, paired t test). We confirmed that ω-
171 CgTx inhibited CA3-CA1 transmission (Figure 2-figure supplement 1) (Wu and Saggau, 1994),
172 suggesting that ω-CgTx we used is effective. In contrast, the application of ω-agatoxin-IVA
173 (ω-Aga-IVA), a P/Q-type Ca^{2+} channel blocker, suppressed both EPSCs and IPSCs to the same
174 extent at SuM-GC synapses (Figure 2B) (EPSC: 23.5 ± 4.6% of baseline, $n = 5$, $p < 0.001$,
175 paired t test; IPSC: 23.9 ± 1.9% of baseline, $n = 6$, $p < 0.05$, Wilcoxon signed-rank test; EPSC
176 vs IPSC: $p = 0.92$, unpaired t test), suggesting that both glutamate and GABA release rely on
177 P/Q-type Ca^{2+} channels at SuM-GC synapses.

178 If the synaptic vesicle pools for glutamate and GABA are identical, the effects of
179 presynaptic G-protein-coupled receptor (GPCR) modulation on both transmissions are
180 expected to be the same. We therefore examined how glutamate/GABA co-transmission is
181 regulated by presynaptic GPCRs. We previously demonstrated that the co-transmission of
182 glutamate and GABA at SuM-GC synapses is presynaptically suppressed by group II
183 metabotropic glutamate receptors (mGluRs) and $GABA_B$ receptors (Hashimotodani et al.,
184 2018). In agreement with this, application of the group II mGluR agonist DCG-IV suppressed
185 both EPSCs and IPSCs at SuM-GC synapses (Figure 2C). Notably, DCG-IV inhibited EPSCs
186 ($IC_{50} = 0.11$ μM) to a greater extent than it did IPSCs ($IC_{50} = 0.27$ μM) (Figure 2C) (two-way

ANOVA, $F_{1,51} = 8.1$, $p < 0.01$). Similar results were found with the application of 5 μM $GABA_B$ receptor agonist baclofen, which suppressed EPSCs more than IPSCs (Figure 2D) (EPSC: 51.6 ± 2.4% inhibition, n = 8; IPSC: 38.6 ± 4.3% inhibition, n = 8, $p < 0.05$, unpaired t test). These differential inhibitory effects of GPCRs on glutamatergic and GABAergic co-transmission are contrary to the expected idea of identical vesicle pools for glutamate and GABA but favor the hypothesis of separate vesicles for glutamate and GABA.

Spatial coupling between presynaptic Ca^{2+} channels and Ca^{2+} sensors of exocytosis is an essential feature in determining the properties of neurotransmitter release, and tight or loose coupling is distinguished by using two different binding rate Ca^{2+} chelators BAPTA and EGTA (Adler et al., 1991; Eggermann et al., 2011). We examined the effects of these two Ca^{2+} chelators on the co-transmission of glutamate and GABA. We found that the bath application of BAPTA-AM suppressed both EPSCs and IPSCs to the same extent (EPSC: 63.4 ± 12.2% of baseline, n = 7, $p < 0.01$, paired t test; IPSC: 63.4 ± 7.8% of baseline, n = 8, $p < 0.001$, paired t test; EPSC vs. IPSC: $p = 0.96$, unpaired t test) (Figure 2E). In contrast, EGTA-AM suppressed EPSCs, whereas it did not affect IPSCs (EPSC: 67.4 ± 7.2% of baseline, n = 6, $p < 0.01$, paired t test; IPSC: 93.1 ± 9.2% of baseline, n = 6, $p = 0.40$, Wilcoxon signed rank test; EPSC vs. IPSC: $p < 0.05$, unpaired t test) (Figure 2E). These results indicate tighter coupling between Ca^{2+} channels and synaptic vesicles for GABA release than for glutamate release.

Minimal light stimulation of SuM inputs elicits independent EPSCs and IPSCs in GCs

Given that light stimulation at normal intensity elicits synchronized release of neurotransmitters from several SuM terminals, it is difficult to evoke a synaptic response mediated by a single vesicle release. For this purpose, we next performed minimal light stimulation to detect stochastic synaptic responses of independent EPSCs and IPSCs, or compound EPSC/IPSC responses (Kim et al., 2022). In this experiment, optical stimulation (over-bouton illumination) was delivered in the presence of tetrodotoxin (TTX) and 4-aminopyridine (4-AP) to exclude SuM inputs-mediated polysynaptic responses, together with D-AP5 to block NMDA receptors. We also decreased the extracellular Ca^{2+} concentration to 1 mM to reduce the release probability. At intermediate holding membrane potentials (–20 to –30 mV), maximum light power illumination elicited biphasic responses (EPSC-IPSC sequence), enabling simultaneous recordings of glutamate/GABA co-transmission in GCs (Figure 3A, left). After confirming the existence of biphasic PSCs, the light power intensity was decreased to detect small synaptic events, that were stochastically observed among the 100 times stimulations (success rate = ~15%) (Figures 3A, 3B, and Figure 3-figure supplement 1). Using

221 this method, we analyzed 1700 trials from 17 cells and detected 86 EPSC-only, 67 IPSC-only,
222 and 19 biphasic events (Figures 3B and 3C). These results indicate that independent EPSCs
223 and IPSCs are the majority of synaptic responses (Figure 3D) (EPSC: 5.1 ± 0.5% probability;
224 IPSC: 3.9 ± 0.4% probability; biphasic: 1.1 ± 0.3% probability, n = 17, EPSC vs biphasic, $p <$
225 0.001; IPSC vs biphasic, $p < 0.001$, one-way ANOVA with Tukey's *post hoc* test). To exclude
226 the possibility that the independent EPSCs and IPSCs detected by minimal light stimulation
227 might have masked the putative tiny synaptic responses of their counterpart currents mediated
228 by the associated transmitters, the amplitudes and kinetics of minimal stimulation-evoked
229 EPSCs and IPSCs were compared with or without blockers of their counterpart receptors. We
230 found that the amplitudes and decay of minimal light stimulation-evoked EPSCs were not
231 changed by the application of the $GABA_A$ receptor blocker picrotoxin (Figure 3-figure
232 supplement 2). Similarly, the amplitudes and rise time of minimal light stimulation-evoked
233 IPSCs were not altered by application of the AMPA/kainate receptor blocker NBQX (Figure
234 3-figure supplement 2). These results validate that EPSCs and IPSCs evoked by minimal
235 optical stimulation are mediated by the stochastic release of glutamate and GABA, respectively,
236 from single vesicles. Furthermore, by comparing minimal stimulation-evoked PSCs with
237 strontium-induced asynchronous PSCs (see below), we found that the amplitudes of EPSCs
238 and IPSCs evoked by minimal stimulation were identical to those of strontium-induced
239 asynchronous EPSCs and IPSCs, respectively (Figure 3G), suggesting that PSCs evoked by
240 minimal stimulation were mediated by a single vesicle release.
241 Taken together, these results indicate that glutamatergic and GABAergic co-transmission
242 occurs independently at SuM-GC synapses.
243
244 **Asynchronous release from SuM terminals exhibits independent EPSCs and IPSCs in**
245 **GCs**
246 It should be noted that minimal light stimulation of SuM inputs may occasionally elicit
247 synchronized release of glutamate and GABA from different vesicle pools, possibly due to the
248 simultaneous opening of several Ca^{2+} channels, which could account for the substantial
249 biphasic responses we detected (Figure 3D). To minimize the likelihood of synchronized
250 release, we recorded asynchronous quantal PSCs by substitution of extracellular Ca^{2+} with Sr^{2+}.
251 At intermediate holding membrane potentials (–20 to –30 mV), light pulses elicited
252 synchronized biphasic responses in the extracellular Ca^{2+} (Figure 3E). By replacing
253 extracellular Ca^{2+} with Sr^{2+}, asynchronous quantal synaptic responses were recorded following
254 light stimulation of the SuM inputs (Figure 3E). By repeating the light stimulation of the SuM

inputs 30 times (every 10 sec), we found that the majority of asynchronous synaptic events were EPSC-only or IPSC-only, whereas biphasic PSCs represented only a minor population (Figures 3F) (EPSC: 27.9 ± 4.7 events; IPSC: 23.4 ± 4.2 events; biphasic: 2.5 ± 0.5 events, n = 11, EPSC vs biphasic, $p < 0.001$; IPSC vs biphasic, $p < 0.001$, one-way ANOVA with Tukey's *post hoc* test). These results further support our conclusion that glutamate/GABA co-transmission is mediated by glutamate and GABA co-released from different populations of synaptic vesicles.

Segregated glutamatergic and GABAergic postsynaptic sites at SuM-GC synapses

We then investigated whether SuM-GC synapses exhibit distinct postsynaptic sites for each neurotransmitter using immunohistochemistry. To enhance spatial resolution, we used ultrathin sections (100-nm-thick) for analysis. As shown previously (Uchigashima et al., 2011), double immunofluorescence revealed that almost all VGluT2-positive terminals in the GC layer co-expressed VIAAT (Figures 4A and 4B). Further post-embedding immunogold EM (Figures 4C and 4D) showed that these terminals formed asymmetric and symmetric synapses, characteristic of excitatory and inhibitory synapses, respectively (Figures 4C and 4D), confirming previous observations (Boulland et al., 2009; Soussi et al., 2010; Root et al., 2018; Billwiller et al., 2020). Conventional EM using serial ultrathin sections also revealed that a single nerve terminal formed both asymmetric and symmetric synapses on a GC soma (Figure 4E). The formation of asymmetric and symmetric synapses by a single SuM terminal was further confirmed by pre-embedding immunogold EM for eYFP, which was expressed in the SuM neurons by injection of AAV-DIO-ChR2(H134R)-eYFP into the SuM of VGluT2-Cre mice (Figure 4F). It has been reported that VTA neurons also project to the GC layer of the DG and co-release glutamate and GABA (Ntamati and Luscher, 2016). However, our retrograde tracing with fluorescent microspheres injected into the dorsal DG did not reveal any retrogradely labeled neurons in the VTA, while labeled neurons were successfully observed in the SuM and entorhinal cortex (EC) (Figure 4-figure supplement 1). This suggests that most of the VGluT2-positive terminals (co-expressed with VIAAT, Figures 4A and 4B) in the GC layer most likely originated from the SuM. To examine the spatial association of SuM terminals with glutamatergic and GABAergic postsynaptic sites, we performed triple immunofluorescence for VGluT2, the NMDA receptor subunit GluN1, and GABAergic postsynaptic sites by the $GABA_A$ receptor subunit $GABA_A\alpha1$. In the GC layer, almost all VGluT2-positive terminals were associated with GluN1 and/or $GABA_A\alpha1$ (Figures 4G and 4H). Specifically, the majority of VGluT2-positive terminals were associated with both GluN1 and $GABA_A\alpha1$ (52.5%), and

289 the remainder were associated with $GABA_A\alpha1$ (22.1%) alone or GluN1 (25.4%) alone (Figure
290 4I). To investigate the spatial relationship between glutamatergic and GABAergic synapses,
291 we quantified the distance between GluN1 and $GABA_A\alpha1$ cluster adjacent to the same
292 VGluT2-positive terminal. On average, the distance was 397.5 ± 8.75 nm, and most VGluT2-
293 positive terminals (79.2%, 191 out of 241) form glutamatergic and GABAergic synapses within
294 500 nm (Figure 4J). Taken together, these results suggest that a single SuM terminal forms
295 GluN1-containing excitatory synapse and $GABA_A\alpha1$-containing inhibitory synapse in separate
296 locations, yet they remain closely proximal.
297
298 **Glutamate/GABA co-transmission balance of SuM inputs is dynamically changed in a**
299 **frequency-dependent manner**
300 The results described thus far indicate that the co-transmission of glutamate and GABA is
301 spatially segregated at SuM-GC synapses, thereby making it possible to independently regulate
302 the co-release of glutamate and GABA from the same SuM terminals. Due to the different
303 release properties of glutamate and GABA in the SuM terminals, glutamate/GABA co-
304 transmission could exhibit different patterns of short-term plasticity at SuM-GC synapses. To
305 test this possibility, we delivered a train of 10 light stimuli at 5-20 Hz, physiologically relevant
306 frequencies (Kirk and McNaughton, 1991; Kocsis and Vertes, 1994; Ito et al., 2018; Farrell et
307 al., 2021), to ChR2-expressing SuM inputs, and compared the short-term depression of EPSCs
308 with that of IPSCs (Figure 5A). To exclude the putative involvement of pre- and/or postsynaptic
309 modulations by mGluRs and $GABA_B$ receptors during a train of stimulation,
310 pharmacologically isolated EPSCs or IPSCs were recorded in the presence of the broad-
311 spectrum mGluR antagonist LY341495 (100 μM) and $GABA_B$ receptor antagonist CGP55845
312 (3 μM). We found that trains of 10 light stimuli at 5, 10, and 20 Hz elicited pronounced short-
313 term synaptic depression of EPSCs during train with stronger depression at higher frequencies
314 (Figures 5A and 5B). We further performed the same experiments under recording conditions
315 with a low release probability by reducing the extracellular Ca^{2+} concentration from 2.5 to 1
316 mM. While train stimulation elicited a weaker depression than 2.5 mM extracellular Ca^{2+},
317 frequency-dependent depression was still observed (Figure 5C). In marked contrast to EPSCs,
318 while IPSCs also exhibited short-term synaptic depression across all tested frequencies,
319 GABAergic co-transmission showed a similar magnitude of depression across all frequencies
320 (Figures 5D and 5E). Similarly, short-term depression of IPSCs did not show a frequency-
321 dependent depression with 1 mM extracellular Ca^{2+} (Figure 5F), leading to a sustained
322 inhibitory effect at any frequency. Given that EPSCs show strong frequency-dependent

depression, whereas IPSCs exhibit frequency-independent sustained depression, it is likely that the EPSC/IPSC ratio can decrease during high-frequency train stimulation. Indeed, comparing the amplitudes of the 10th EPSCs with those of the 10th IPSCs indicated that the depression of EPSCs was stronger than that of IPSCs at 10 Hz and 20 Hz (Figure 5G). We further addressed whether short-term dynamic changes in the EPSC/IPSC ratio could be observed in the same cell by recording the biphasic synaptic responses at intermediate membrane potentials that enabled simultaneous monitoring of the compound EPSC/IPSC. We found that 10 Hz train light illumination induced a stronger depression of EPSCs than of IPSCs (Figure 5-figure supplement 1), thereby decreasing the EPSC/IPSC ratio during the high-frequency train stimulation. We confirmed that the fiber volley induced by trains of 10 light stimuli was comparable across all tested frequencies (Figure 5-figure supplement 2), indicating that a similar number of SuM fibers were activated with each light pulse during trains.

Despite the differential properties of the co-release of glutamate and GABA from SuM terminals, the difference in the magnitude of short-term depression between glutamatergic and GABAergic co-transmission could be mediated by postsynaptic mechanisms, such as AMPA receptor saturation and desensitization during burst high-frequency stimulation (Trussell et al., 1993; Brenowitz and Trussell, 2001; Heine et al., 2008). To test this possibility, we recorded EPSC trains in the presence of γ-D-glutamylglycine (γDGG), a low-affinity AMPA receptor antagonist that relieves AMPA receptor saturation and desensitization (Wadiche and Jahr, 2001; Wong et al., 2003; Foster and Regehr, 2004). As expected, 2 mM γDGG reduced the amplitude of EPSCs (60.1 ± 4.3% reduction, $n = 16$, $p < 0.001$, paired t test). Under these conditions, short-term depression with high-frequency light stimulation (10 Hz and 20 Hz) was not affected (Figure 5-figure supplement 3A, B). This rules out a postsynaptic contribution to the strong depression of EPSCs and suggests that presynaptic mechanisms mediate this short-term depression. Similarly, to determine whether postsynaptic $GABA_A$ receptor saturation is involved in short-term depression during train stimulation, we used the low-affinity competitive $GABA_A$ receptor antagonist TPMPA (Sakaba, 2008; Markwardt et al., 2009; Turecek et al., 2016). We found that 300 μM TPMPA reduced the amplitude of IPSCs (47.1 ± 3.8% reduction, $n = 11$, $p < 0.01$, Wilcoxon signed rank test), while short-term depression of IPSCs in response to 10 light pulses at 10 Hz and 20 Hz did not differ before and after the application of TPMPA (Figure 5-figure supplement 3C, D), excluding the involvement of $GABA_A$ receptor saturation in the short-term depression of IPSCs at SuM-GC synapses, suggesting a presynaptic origin of this short-term plasticity.

Taken together, these results suggest that SuM-GC synapses exhibit short-term dynamic changes in the glutamate/GABA co-transmission ratio during repetitive high-frequency SuM activity due to the different properties of frequency-dependent depression between glutamatergic and GABAergic transmission, favoring inhibition over excitation. Furthermore, the different properties of short-term depression of EPSCs and IPSCs also support the segregated co-transmission of glutamate and GABA at SuM-GC synapses.

SuM inputs modulate GC activity in a frequency dependent manner

We have previously demonstrated that SuM inputs associated with EC inputs facilitate GC firing (Hashimotodani et al., 2018). Our previous study investigated the single association of synaptic inputs, but did not examine repetitive stimulation of synaptic inputs. We investigated how the repetitive activation of SuM inputs, which implement frequency-dependent filtering of glutamatergic responses with sustained synaptic inhibition by GABAergic co-transmission, affects GC excitability. To mimic excitatory EC synaptic inputs onto GCs, a sinusoidal current was injected into the soma of GCs (Kamondi et al., 1998; Magee, 2001; Ajibola et al., 2021), which can bypass direct synaptic stimulation of the perforant path (main excitatory inputs originating from EC) and, consequently, circumvent the recruitment of inhibitory circuitry. We found that a sinusoidal current at 5 Hz generated action potentials at the peak of the depolarizing phase (Figure 6A). The injected current was adjusted to generate action potentials with fewer than five spikes in each trial (10 cycles), and the optogenetically activated SuM inputs were paired at the depolarizing phase of each cycle. Paired light illumination significantly enhanced GC firing compared to sinusoidal current injections without light stimulation throughout the trial (10 stimuli) (Figures 6A and 6D). Notably, the probability of spikes further increased when GABAergic transmission was blocked by picrotoxin (Figures 6A and 6D). These results suggest that SuM inputs enhance GC firing and that GABAergic co-transmission negatively regulates the net excitatory effect of SuM inputs at 5 Hz, similar to the effects of a single associational activation of SuM and EC inputs (Hashimotodani et al., 2018). In striking contrast, at higher frequencies (10 Hz and 20 Hz), the enhancement of spike probability by SuM activation was attenuated and disappeared in the last few stimulations (Figures 6B, 6C, 6E, and 6F). Importantly, in the presence of picrotoxin, SuM activation by light stimulation enhanced GC firing, even in the last few stimulations (Figures 6B, 6C, and 6E, 6F), suggesting that SuM glutamatergic co-transmission still exerted excitatory effects in the later cycle, even during the short-term depression of glutamate release. Thus, the excitatory action of SuM inputs was filtered by the co-released GABA during repetitive high-frequency

stimulation due to frequency-independent sustained depression. These results indicate that SuM inputs modulate GC output in a frequency-dependent manner due to the different short-term plasticities of glutamate/GABA co-transmission.

Discussion

Despite evidence that glutamate and GABA are co-released from the synaptic terminals of a subset of neurons in the adult brain, whether glutamate and GABA are released from the same or distinct synaptic vesicle populations remains a debate (Shabel et al., 2014; Root et al., 2018; Kim et al., 2022). In this study, we demonstrate that the transmission properties of glutamate and GABA at SuM-GC synapses differ in PPR, Ca^{2+}-sensitivity, presynaptic GPCR regulation, and Ca^{2+} channel-synaptic vesicle coupling configuration. We further found that uniquantal synaptic responses exhibit independent EPSCs and IPSCs. The anatomical results show that a single SuM terminal forms both asymmetric and symmetric synapses with a GC soma. The postsynaptic excitatory site (marked by GluN1) and inhibitory site (marked by $GABA_A\alpha1$), facing the same SuM terminal, are closely positioned but distinct. These findings provide evidence that glutamatergic and GABAergic co-transmission occurs at functionally distinct release sites (Figure 7). Owing to the functional and spatial segregation of the co-transmission of glutamate and GABA, each transmission exhibits distinct short-term plasticities, leading to different frequency-dependent effects of SuM inputs on the GC activity.

Different release properties of dual-neurotransmitter neurons have been reported in other synaptic circuits. Different PPRs (Lee et al., 2010; Silm et al., 2019; Zych and Ford, 2022) and Ca^{2+}-sensitivities (Lee et al., 2010; Zych and Ford, 2022) between co-transmission of dual-neurotransmitters are found in the retina (acetylcholine and GABA) and striatum (dopamine and glutamate or GABA). Different reliance on Ca^{2+} channels for distinct neurotransmitters have been reported in the retina (acetylcholine and GABA) (Lee et al., 2010), striatum (dopamine and glutamate) (Silm et al., 2019), and hippocampus (acetylcholine and GABA) (Takacs et al., 2018). These differential release properties of the two neurotransmitters indicate a separate release from distinct vesicle pools (Lee et al., 2010; Takacs et al., 2018; Silm et al., 2019). Our study also demonstrated that glutamate and GABA co-release from SuM terminals shows differences in PPR and Ca^{2+}-sensitivity. Glutamatergic transmission exhibited a stronger depression than GABAergic transmission, suggesting that release probability of glutamate is higher than that of GABA. A higher reduction in IPSCs than EPSCs by decreasing the extracellular Ca^{2+} concentration from 2.5 to 1 mM indicates that GABA release requires higher extracellular Ca^{2+} than glutamate release. Furthermore, using the Ca^{2+} chelators BAPTA and

424 EGTA, we found that the spatial coupling between Ca^{2+} channels and synaptic vesicles of
425 GABA is tighter than that of glutamate. These differences in release properties can be attributed
426 to the different compositions of the release machinery and different spatial organizations
427 between the release machinery and Ca^{2+} channels for glutamate and GABA release (Sudhof,
428 2013; Neher and Brose, 2018). Given that GABAergic co-transmission exhibits a lower release
429 probability and a higher requirement for extracellular Ca^{2+}, together with tight coupling
430 between Ca^{2+} channels and vesicles, synaptic vesicles for GABA release could be surrounded
431 by a few Ca^{2+} channels in close proximity. In contrast, the synaptic vesicles for glutamate
432 release could be surrounded by a large number of Ca^{2+} channels at longer distances than those
433 for GABA release. As with other possible mechanisms, the different expression of transporters
434 in the vesicles with their interacting proteins may contribute to different release probabilities.
435 Given that VGluT1 and endophilin interaction exhibits different release probabilities compared
436 to VGluT2-expressing synapses (Weston et al., 2011), it is postulated that different interactions
437 of VGluT2 and VIAAT with their different binding proteins could determine distinct release
438 probabilities.
439 How are VGluT2 and VIAAT sorted into the distinct synaptic vesicles, and how are
440 glutamate vesicles and GABA vesicles sorted to different places within the same SuM
441 terminal? With synaptic vesicles containing 410 different proteins (Takamori et al., 2006), even
442 slight differences in molecular composition or incorporation of specific molecules on the
443 vesicles could influence their functional properties (Chamberland and Toth, 2016). These
444 differences may determine the selective sorting of neurotransmitter transporters into vesicles
445 and the precise arrangement of glutamate and GABA vesicles at the distinct active zones within
446 the same terminal. Especially, VGluT2 and VIAAT contain sorting motifs in their C-terminus,
447 which interacts with clathrin adaptor proteins (APs). Several studies demonstrated that the
448 interaction between neurotransmitter transporters and APs is important for endocytosis and
449 recycling of synaptic vesicles (Nakatsu et al., 2004; Voglmaier et al., 2006; Santos et al., 2013;
450 Li et al., 2017; Silm et al., 2019). Distinct APs-dependent recycling pathway may contribute to
451 formation of precise spatial localization of glutamate and GABA vesicles in the same SuM
452 terminal (Asmerian et al., 2024). Our immuno-EM analysis showed that VGluT2 and VIAAT
453 appear to be randomly distributed in the terminal (Figures 4C and 4D). However, it is important
454 to acknowledge that due to low labeling efficiency, our immuno-EM images may not capture
455 the full spectrum of synaptic vesicles for glutamate and GABA. It is known that synaptic
456 vesicles are divided into three categories: the readily releasable pool (RRP), recycling pool,
457 and resting pool (Alabi and Tsien, 2012; Miki et al., 2022). Among them, the vast majority of

458 synaptic vesicles (~85% of the total vesicles) belongs to the resting pool. Therefore, it is likely
459 that most of the VGluT2 and VIAAT labeling corresponds to the synaptic vesicles in the resting
460 pool. Further studies are necessary to investigate whether VGluT2-containing vesicles and
461 VIAAT-containing vesicles in the RRP and recycling pools, both of which are closely linked
462 to exocytosis, are clearly segregated near their respective active zones.

463 Our data showed that both glutamate and GABA release rely on P/Q-type Ca^{2+} channels at
464 SuM-GC synapses. Interestingly, the excitatory transmission of SuM-CA2 pyramidal neuron
465 synapses, an exclusive glutamatergic synapse (Chen et al., 2020), is also mediated by P/Q-type
466 Ca^{2+} channels (Robert et al., 2021). Therefore, neurotransmitter release from SuM neurons
467 depends on P/Q-type Ca^{2+} channels, irrespective of the target neurons. We found that the
468 activation of group II mGluRs and $GABA_B$ receptors inhibited glutamatergic co-transmission
469 more strongly than GABAergic co-transmission. Given that these GPCRs suppress presynaptic
470 Ca^{2+} channels via $G_{i/o}$-protein, and that both transmitter releases are mediated by the same type
471 of Ca^{2+} channels, the different extents of inhibition of the co-release of glutamate/GABA by
472 group II mGluRs and $GABA_B$ receptors may be attributed to differential expression levels of
473 receptors or signaling efficacy between glutamate and GABA release. Additionally, the spatial
474 coupling between GPCRs and active zones for glutamate and GABA in the same SuM
475 terminals may be different, which may give rise to differential modulation of glutamate and
476 GABA release.

477 Consistent with previous EM studies (Boulland et al., 2009; Soussi et al., 2010; Root et al.,
478 2018; Billwiller et al., 2020), we found that a single SuM terminal forms symmetric and
479 asymmetric synapses in the DG (Figures 4E and 4F). However, confirming whether these
480 synapses function as glutamatergic or GABAergic relies on the identification of their
481 postsynaptic receptors, which remains unresolved. In our study, we demonstrated that both
482 GluN1 and $GABA_A\alpha1$ were associated with common SuM terminals (Figures 4G and 4H),
483 suggesting that these synapses represent distinct glutamatergic and GABAergic synapses.
484 Furthermore, our analysis showed that approximately 50% of SuM terminals was associated
485 with both GluN1 and $GABA_A\alpha1$ (Figure 4I). It should be noted, however, this percentage can
486 be an underestimate due to the utilization of 100-nm-thick ultrathin sections, which limits the
487 detection of co-localization events within this confined spatial range. Consequently, the actual
488 percentage is expected to be significantly higher. Hence, the predominant synapse type of SuM
489 terminals consists of dual glutamatergic and GABAergic synapses, with additional individual
490 glutamatergic or GABAergic synapses.

Previous electrophysiological studies have demonstrated that both glutamate and GABA are co-packaged in the same synaptic vesicles in the lateral habenula (Shabel et al., 2014; Kim et al., 2022). Minimal optogenetic stimulation of EP terminals evoked a high proportion of biphasic PSCs over independent EPSCs and IPSCs in lateral habenular neurons, suggesting the co-release of glutamate and GABA from the same synaptic vesicles (Kim et al., 2022). While these findings appear to contradict anatomical data showing distinct populations of glutamate- and GABA-containing synaptic vesicles in the lateral habenula (Root et al., 2018), technical limitations of immuno-EM may affect the ability to accurately assess the spatial distributions of proteins within the vesicles (Kim and Sabatini, 2023). Such limitations include antibody interference on small vesicles, restricted access to target molecules, and the stochastic nature of labeling two molecules in a single vesicle. In addition, the existence of VTA terminals, other glutamate/GABA co-release inputs (Root et al., 2014; Yoo et al., 2016; Root et al., 2018), may complicate the interpretation of the co-release mechanisms in the lateral habenula. In contrast, in the DG, we found that the majority of synaptic responses evoked by both minimal light stimulation and asynchronous release at SuM-GC synapses showed independent EPSCs and IPSCs. A previous biochemical study detected VGluT2 and VIAAT in distinct purified synaptic vesicles from the hippocampus (Boulland et al., 2009). Moreover, differences in transport mechanisms between glutamatergic and GABAergic vesicles have been reported (Farsi et al., 2016). Based on this evidence, our results most likely support the hypothesis that glutamate and GABA are packaged in distinct synaptic vesicles (Figure 7). Thus, glutamate/GABA co-transmission is diverse, in that both transmitters are co-released from the same or different synaptic vesicles, depending on brain regions and synapse types. It is important to note that transmitter release is detected by postsynaptic receptors; therefore, even if two neurotransmitters are co-released from the same vesicles, they will not be detected unless the postsynaptic targets express receptors for both (Dugue et al., 2005; Granger et al., 2020). Accordingly, while our results strongly suggest that glutamate/GABA co-transmission occurs independently at segregated excitatory and inhibitory SuM-GC synapses, it remains possible that glutamate and GABA are co-released from the same vesicles, with one transmitter undetected due to the absence of its postsynaptic receptor. Further study will be necessary to determine the packaging mechanisms of glutamate and GABA within SuM terminals.

The distinct co-transmission modes of the two transmitters have the ability to exert independent synaptic regulation compared with their co-release from identical vesicles. At SuM-GC synapses, we demonstrated that glutamatergic and GABAergic co-transmission exhibited different short-term plasticities. While glutamatergic co-transmission showed strong

frequency-dependent depression, GABAergic co-transmission exhibited stable frequency-independent depression. By this frequency-specific dynamic change of the glutamate/GABA co-transmission balance, at low-frequency burst SuM inputs, they operated as excitatory inputs, whereas at high frequency, the excitatory effects of SuM inputs on GCs were inhibited by co-transmitted GABA (Figure 6). Accordingly, GCs respond differently to SuM inputs in a frequency-dependent manner, due to the low-pass filtering of SuM-GC synapses. The fact that the theta-rhythm in the hippocampus is associated with synchronized SuM activity (Kirk and McNaughton, 1991; Kocsis and Vertes, 1994; Ito et al., 2018; Farrell et al., 2021) has important implications for the low-pass filtering of this synapse. As SuM inputs act as excitatory at 5 Hz (theta) train stimulation, but not at higher frequencies, SuM inputs may transfer their train information exclusively at the theta frequency, which could contribute to theta-mediated information processing in SuM-hippocampal circuits and their relevant brain functions, including cognitive, sleep, and navigation processes (Pedersen et al., 2017; Billwiller et al., 2020; Chen et al., 2020; Li et al., 2020; Farrell et al., 2021; Kesner et al., 2023). In addition to SuM inputs, GCs receive EC inputs as the main excitatory inputs for discharge, and other excitatory inputs from hilar mossy cells (Hashimotodani et al., 2017). Therefore, low-pass filtering of SuM inputs could prevent the over-excitation of GCs, leading to anti-seizure effects. In contrast to the presynaptic origin of short-term plasticity at SuM-GC synapses, we previously demonstrated the postsynaptically induced long-term potentiation at SuM-GC synapses, which selectively occurs of glutamatergic co-transmission (Hirai et al., 2022; Tabuchi et al., 2022). Our findings suggest that SuM inputs play diverse roles in modulating GC output via short- and long-term plasticity with pre- and postsynaptic distinct mechanisms, respectively.

Materials and Methods

Animals

C57BL/6 and VGluT2-Cre mice (Jackson Labs, Slc17a6$^{tm2(cre)Lowl}$/J, stock #016963) of either sex aged 6–7 weeks were used for electrophysiological experiments and male C57BL/6 mice at 2–3 months of age were used for anatomical experiments (Figure 4). All animals were group housed in a temperature- and humidity-controlled room under a 12 hr light/12 hr dark cycle. Water and food were provided *ad libitum*. The experiments were approved by the animal care and use committee of Doshisha University and Hokkaido University and were performed in accordance with the guidelines of the committees.

560

561 **Stereotaxic injections**

562 Mice on postnatal days 19 to 21 were placed in a stereotaxic frame, and anesthetized with
563 isoflurane (1.5–2.5%). A beveled glass capillary pipette connected to a microsyringe pump
564 (UMP3, WPI) was used for the viral injection. 200 nL of AAV1-EF1a-DIO-hChR2(H134R)-
565 eYFP (Addgene) was injected into the SuM (relative to bregma, AP: –2.2 mm, ML: ±0.5 mm,
566 DV: –4.85 mm) at a rate of 50 nL/min. The glass capillary was remained at the target site for
567 5 min before the beginning of the injection and was removed 10 min after infusion. For
568 retrograde tracing, 900 nL of 0.8 % fluorescent microspheres (Fluospheres, 0.04 μm, 565/580,
569 Invitrogen, F8794) was injected unilaterally into the dorsal DG (relative to bregma, AP: – 1.96
570 mm, ML: 1.484 mm, DV: 1.93 mm) at a rate of 100 nL/min using a 10 μl Hamilton
571 microsyringe with a beveled 32 gauge needle. Animals were sacrificed two weeks later for
572 fluorescent retrograde tracing.

573

574 **Hippocampal slice preparation**

575 Acute transverse hippocampal slices (300-μm-thick) were prepared from mice 3–4 weeks after
576 AAV injection. The mice were decapitated under isoflurane anesthesia. Briefly, the hippocampi
577 were isolated, embedded in an agar block, and cut using a vibratome (VT1200S, Leica
578 Microsystems) in an ice-cold cutting solution containing (in mM): 215 sucrose, 20 D-glucose,
579 2.5 KCl, 26 $NaHCO_3$, 1.6 NaH_2PO_4, 1 $CaCl_2$, 4 $MgCl_2$, and 4 $MgSO_4$. Brain blocks, including
580 the interbrain and midbrain, were also isolated and fixed in 4% paraformaldehyde (PFA) for
581 *post hoc* our internal check of the injection site (Tabuchi et al., 2022). Hippocampal slices were
582 transferred to an incubation chamber and incubated at 33.5°C in the cutting solution. After 30
583 min of incubation, the cutting solution was replaced with an extracellular artificial
584 cerebrospinal fluid (ACSF) containing (in mM): 124 NaCl, 2.5 KCl, 26 $NaHCO_3$, 1 NaH_2PO_4,
585 2.5 $CaCl_2$, 1.3 $MgSO_4$ and 10 D-glucose at 33.5°C. The slices were stored at room temperature
586 for at least 1 h before recording. Both the cutting solution and the ACSF were oxygenated with
587 95% O_2 and 5% CO_2. After recovery, slices were transferred to a submersion-type recording
588 chamber for electrophysiological analysis.

589

590 **Electrophysiology**

591 Whole-cell recordings using an EPC10 (HEKA Electronik) or IPA amplifier (Sutter
592 Instruments) were made from GCs using an infrared differential interference contrast
593 microscopy (IR-DIC, Olympus, BX51WI). We recorded from GCs with an input resistance of

< 300 MΩ for mature GCs (Schmidt-Hieber et al., 2004). The data were filtered at 2.9 kHz and sampled at 20 kHz. For voltage-clamp recordings, we used patch pipettes (3–6 MΩ) filled with an intracellular solution with the following composition (in mM): 131 Cs-gluconate, 4 CsCl, 10 HEPES, 0.2 EGTA, 2 Mg-ATP, 0.3 Na_3GTP, 10 phosphocreatine, pH 7.3 adjusted with CsOH (the calculated E_{Cl-} = –90 mV) (292–300 mOsm). In some experiments, biocytin (0.5 %) was included in the intracellular solution for morphological visualization of GCs after recording using Alexa Fluor 568-conjugated streptavidin (1:500, Thermo Fisher Scientific). For recordings of synaptic currents at intermediate membrane potentials, 5 mM QX314 was included in the intracellular solution. ChR2-expresing SuM fibers were activated at 0.05 Hz by a pulse of 470 nm blue light (1–5 ms duration, 5.0–10.5 mW/mm^2) delivered through a ×40 objective attached to a microscope using an LED (Mightex or ThorLabs). The light intensity was adjusted to yield less than 80% of the maximum response during the baseline period. The illumination field was centered over the recorded cell, unless otherwise stated. Series resistance (8–20 MΩ) was uncompensated and monitored throughout experiments with a –5 mV, 50 ms voltage step, and cells that exhibited a significant change in the series resistance more than 20% were excluded from analysis.

For minimal light stimulation experiments, we first recorded biphasic synaptic responses from GCs by maximum light stimulation of SuM inputs at intermediate membrane potentials from –20 to –30 mV in the presence of 1 μM TTX, 1 mM 4-AP, 50 μM D-AP5, and 1 mM Ca^{2+}. The exact membrane potentials were set to the potential at which the amplitudes of EPSCs and IPSCs were similar. Then, light power intensity was decreased to detect small stochastic synaptic events. We adjusted the light power (<1 ms duration, <1.0 mW/mm^2) to evoke synaptic responses, with a success rate of 15%. A total of 100 trials were recorded every 10 s. EPSC-only responses were determined as the synaptic current with the onset of a downward deflection within 6 ms of light illumination that returned to the baseline without an outward current within 20 ms of light illumination. IPSC-only responses were determined as the synaptic current with the onset of an upward deflection within 6 ms of light illumination, without an inward current immediately after light illumination. Biphasic responses were defined as an EPSC-IPSC sequence, only if an outward peak current following an inward current appeared within 20 ms of light illumination. The amplitude threshold was set to three times the SD of the baseline noise. Based on these criteria, we confirmed that the detection rate of false-positive events (without light illumination) was 0.6 ± 0.4% (3/500 trials, n = 5).

For recordings of asynchronous synaptic events, we initially recorded light stimulation-evoked biphasic synaptic responses at intermediate membrane potentials (–20 to –30 mV) in

628 the presence of Ca^{2+}. The ACSF was then replaced with Ca^{2+}-free ACSF containing 4 mM
629 $SrCl_2$. Asynchronous synaptic responses were evoked by light pulses at 0.1 Hz for 30 times,
630 measured during a 450 ms period beginning 30 ms after the stimulus to exclude the initial
631 synchronous synaptic responses, and analyzed using the Mini Analysis Program (Synaptosoft).
632 D-AP5 (50 μM) was included in the extracellular ACSF throughout the experiment to eliminate
633 NMDA receptor-mediated currents.
634 For train stimulation, EPSCs were recorded from GCs at a holding potential of –70 mV in
635 the presence of 100 μM picrotoxin, while IPSCs were recorded at a holding potential of 0 mV
636 in the presence of 10 μM NBQX and 50 μM D-AP5. Biphasic PSCs were recorded at a holding
637 potential of –30 mV in the presence of 1 μM TTX, 500 μM 4-AP, and 50 μM D-AP5. In all
638 train-stimulation experiments, 100 μM LY341495 and 3 μM CGP55845 were also added to the
639 ACSF throughout the experiments. 10 light pulses at 5 Hz, 10 Hz, and 20 Hz were delivered
640 every 20 sec, and 10–20 sweeps were recorded.
641 For field potential recordings in the CA1 region, a recording pipette filled with 1 M NaCl
642 and a patch pipette with broken tip (with diameter of ~20–30 μm) filled with the ACSF were
643 placed in the stratum radiatum of the CA1 region. For recordings of the fiber volley originating
644 from ChR2-epressing SuM fibers, a recording pipette was placed in the supragranular layer
645 where ChR2-epressing SuM fibers were densely distributed. Light-evoked field potentials were
646 recorded in the presence of 10 μM NBQX, 50 μM D-AP5, and 100 μM picrotoxin to block the
647 synaptic responses.
648 For current-clamp recordings, we used an intracellular solution with the following
649 composition (in mM): 135 $KMeSO_4$, 5 KCl, 10 HEPES, 0.2 EGTA, 2 MgATP, 0.3 Na_3GTP, 10
650 phosphocreatine, pH 7.3 adjusted with NaOH (the calculated E_{Cl-} = –82 mV) (297–299 mOsm).
651 A sinusoidal current was delivered to the soma of GCs at 5 Hz, 10 Hz, and 20 Hz (10 cycles),
652 while the membrane potential was held at -70 mV to -80 mV. The injected current (100–240
653 pA) was adjusted to generate action potentials with fewer than five spikes in each trial. After
654 obtaining control, a sinusoidal current injection was paired with light stimulation of SuM inputs
655 at the depolarizing phase of each cycle. Subsequently, 100 μM picrotoxin was bath applied,
656 and the same pairing of sinusoidal current with light stimulation were delivered. In each
657 experiment, 10 trials were recorded every 20 sec.
658 All experiments were performed at 30–33°C in the recording chamber perfused (2
659 mL/min) with oxygenated ACSF.
660
661 **Pharmacology**

662 Each reagent was dissolved in water, NaOH or DMSO, depending on the manufacture's
663 recommendation to prepare a stock solution, and stored at –20°C. NBQX, D-AP5, (R)-baclofen,
664 DCG-IV, γDGG, TPMPA, and LY341495 were purchased from Tocris Bioscience. ω-
665 Conotoxin GVIA and ω-agatoxin IVA were purchased from the Peptide Institute. Picrotoxin
666 was purchased from the Tokyo Chemical Industry. 4-AP and BAPTA-AM were purchased from
667 nacalai tesque. TTX was purchased from Fujifilm Wako Pure Chemical. EGTA-AM was
668 purchased from AAT Bioquest. CGP55845 was purchased from Hello Bio. Reagents were bath
669 applied following dilution into ACSF from the stock solutions immediately before use.
670

671 **Antibodies**

672 Primary antibodies raised against the following molecules were used: $GABA_A$ receptor α1
673 subunit, NMDA receptor GluN1 subunit, VGluT2, VIAAT, and GFP. Information on the
674 molecule, antigen sequence, host species, specificity, reference, NCBI GenBank accession
675 number, and RRID of the primary antibodies used is summarized in Table S1.
676

677 **Immunohistochemistry for ChR2-expressing SuM terminals**

678 Under deep pentobarbital anesthesia (100 mg/kg of body weight, intraperitoneally), AAV-DIO-
679 ChR2(H134R)-eYFP injected VGluT2-Cre mice were perfused with 4% PFA. Brains were
680 removed and stored in 4% PFA for 4 h at room temperature, then transferred to PBS and left
681 overnight at 4°C. Coronal brain slices containing the SuM or the hippocampus were sectioned
682 at 100 μm using a vibratome (VT1200S, Leica microsystems). After permeabilization in PBS
683 with 1% Triton X-100 for 30 min, the sections were blocked in PBS with 5% donkey serum
684 for 1h. After washing three times with PBS for 10 min each, the sections were incubated in
685 PBS containing primary antibodies and 0.5% Triton X-100 overnight at room temperature.
686 Primary antibodies against GFP (goat, 1:200), VGluT2 (rabbit, 1:200), and VIAAT (guinea pig,
687 1:200) were used. The sections were then rinsed with PBS three times, and incubated in PBS
688 containing 0.5% Triton X-100 and secondary donkey antibodies (1:500, anti-goat Alexa Fluor
689 488-conjugated antibody, abcam, ab150129; anti-rabbit Alexa Fluor 568-conjugated antibody,
690 abcam, ab175470; anti-guinea pig Cy5-conjugated antibody, Jackson ImmunoResearch, 706-
691 175-148) for 2h at room temperature. Sections were rinsed three times in PBS and mounted on
692 glass slides with DAPI. To analyze colocalization of ChR2-eYFP-labeled axonal boutons with
693 VGluT2 and VIAAT, z stack images were captured (0.4 μm optical sections) using a
694 fluorescence microscope (BZ-X800, Keyence). Swellings of ChR2-YFP labeled axons were
695 considered as axonal boutons, and their colocalization with VGluT2 and VIAAT

immunofluorescence was examined in 3D planes as previously reported (Hashimotodani et al., 2018).

Immunofluorescence using ultrathin sections

Under deep pentobarbital anesthesia (100 mg/kg body weight, i.p.), mice were fixed by transcardially with 5 ml of saline, followed by 60 ml of glyoxal fixative solution (9% glyoxal [Sigma], 8% acetic acid, pH 4.0) (Konno et al., 2023). Brains were dissected and post-fixed at 4°C in glyoxal fixative solution for 2 hr. Coronal 400-µm-thick brain sections were cut on a vibratome (VT1000S, LeicaMicrosystems). Sections were embedded in durcupan (Sigma) and ultra-thin sections (100-nm-thick) were prepared by Ultracut ultramicrotome (Leica Microsystems). Sections were mounted on silane-coated glass slides (New Silane II, *Muto* Pure Chemicals). After etching with saturated sodium ethanolate solution for 1–5 s, ultra-thin sections on slides were treated with ImmunoSaver (Nisshin EM) at 95°C for 30 min. Sections were blocked with 10% normal donkey serum (Jackson ImmunoResearch) for 20 min, then incubated with a mixture of primary antibody solution (1 µg/ml in phosphate-buffered saline (pH 7.2) containing 0.1% TritonX-100 (PBST) overnight at room temperature. Sections were washed three times with PBST and incubated with a solution of Alexa488, Cy3, and Alexa647-labeled species-specific secondary antibodies (Jackson ImmunoResearch; Thermo Fisher Scientific) diluted at 1:200 in PBST for 2 h at room temperature. After washing, sections were air-dried and mounted using ProLong Glass (Thermo Fisher Scientific). Photographs were taken with a confocal laser microscope (FV1200, Evident) using 20x and 60x objectives.

Conventional electron microscopy

Under deep anesthesia with pentobarbital (100 mg/kg, i.p.), mice were transcardially perfused with 2% PFA/2% glutaraldehyde in 0.1 M PB (pH 7.2) for 10 min, and the brains were removed. Brains were then postfixed for 2 h in the same fixative, and coronal sections (50-µm-thick) were prepared using a vibratome (VT1000S, Leica Microsystems). Sections were fixed with 1% osmium tetroxide solution for 15 min, and then stained with 2% uranyl acetate for 15 min, dehydrated in a graded ethanol series and n-butyl glycidyl ether, embedded in epoxy resin, and polymerized at 60 °C for 48 h. Ultrathin sections (~80-nm-thick) were prepared with an ultramicrotome (UCT7, Leica Microsystems). Serial sections were mounted on indium-tin-oxide-coated glass slides (IT5-111-50, NANOCS) and successively stained with 2% uranyl acetate and lead citrate. After washing, colloidal graphite (Ted Pella Inc) was pasted on the glass slides to surround the ribbons. Images were acquired using a SEM with a backscattered electron beam detector at an accelerating voltage of 1.0 kV and a magnification of ×12,000 (SU8240, Hitachi High Technologies).

732

733 **Postembedding immunoelectron microscopy**

734 Under deep anesthesia with pentobarbital (100 mg/kg, i.p.), mice were transcardially perfused
735 with 4% PFA/0.1 M PB (pH 7.2) for 10 min, brains were removed, postfixed for 2 h in the
736 same fixative, and coronal sections (400-μm-thick) prepared using a vibratome (VT1000S,
737 Leica Microsystems). Then, sections were cryoprotected with 30% glycerol in PB, and frozen
738 rapidly with liquid propane in the EM CPC unit (Leica Microsystems). Frozen sections were
739 immersed in 0.5% uranyl acetate in methanol at –90°C in the AFS freeze-substitution unit
740 (Leica Microsystems), infiltrated at –45°C with Lowicryl HM-20 resin (Chemische Werke
741 Lowi, Waldkraiburg, Germany), and polymerized with ultraviolet light. Ultrathin sections were
742 made using an Ultracut ultramicrotome (Leica Microsystems). Ultrathin sections (100-nm-
743 thick) mounted on nickel grids were etched with ultrathin sections on nickel grids were etched
744 with saturated sodium-ethanolate solution for 1–5 s. For double labeling against VGluT2 and
745 VIAAT, sections were incubated in blocking solution containing 2% normal goat serum
746 (Nichirei, Tokyo, Japan) in 0.03% Triton X-100 in Tris-buffered saline (TBST, pH 7.4),
747 followed by VIAAT antibody (20 μg/ml) diluted in 2% normal goat serum in TBST overnight,
748 then colloidal gold-conjugated (5 nm) anti-rabbit IgG in blocking solution for 2 hr. After
749 extensive washing in distilled water, sections were incubated in blocking solution containing
750 2% rabbit serum (Nichirei, Tokyo, Japan) in TBST for 10 min, VGluT2 antibody (20 μg/ml)
751 diluted with 2% normal rabbit serum in TBST overnight, and colloidal gold-conjugated (10
752 nm) anti-guinea pig IgG in blocking solution for 2 hr. After extensive washing in distilled water,
753 sections were fixed with 2% OsO4 for 15 min, then stained with 5% uranyl acetate/40% EtOH
754 for 90 s and Reynold's lead citrate solution for 60 s. Photographs were taken from the granular
755 layer of the dentate gyrus with an H-7100 electron microscope at x20,000 magnification.

756

757 **Pre-embedding immunoelectron microscopy**

758 Under deep anesthesia with pentobarbital (100 mg/kg, i.p.), VGluT2-Cre mice, in which
759 AAV1-EF1a-DIO-hChR2(H134R)-eYFP was injected into the SuM were transcardially
760 perfused with 4% PFA/0.1 M PB (pH 7.2) for 10 min, and the brains were removed. Brains
761 were then postfixed for 2 h in the same fixative, and coronal sections (50-μm-thick) were
762 prepared using a vibratome (VT1000S, Leica Microsystems). PBS (pH 7.4) containing 0.1%
763 Tween 20 was used as incubation and washing buffer. Sections were blocked with 10% normal
764 goat serum (Nichirei Bioscience Corporation) for 20 min and incubated with rabbit anti-GFP
765 antibody (1 μg/ml) overnight at room temperature. After washing, sections were incubated with
766 colloidal-conjugated anti-rabbit IgG (1:100; Nanoprobes) for 2h at room temperature. Sections

767 were washed with HEPES Buffer (50 mM HEPES, 200 mM sucrose, 5 N sodium hydroxide)
768 (pH 8.0), and then incubated with silver enhancement reagent (AURION R-Gent SE-EM;
769 AURION) for 1 h. Sections were fixed with 1% osmium tetroxide solution on ice for 15 min,
770 and then stained with 2% uranyl acetate for 15 min, dehydrated in a graded ethanol series and
771 n-butyl glycidyl ether, embedded in epoxy resin, and polymerized at 60 °C for 48 h. Ultrathin
772 sections (~80-nm-thick) in the plane parallel to the section surface were prepared with an
773 ultramicrotome (UCT7, Leica Microsystems). Serial sections were mounted on indium-tin-
774 oxide-coated glass slides (IT5-111-50, NANOCS) and successively stained with 2% uranyl
775 acetate and lead citrate. After washing, colloidal graphite (Ted Pella Inc) was pasted on the
776 glass slides to surround the serial sections. Images were acquired using a SEM with a
777 backscattered electron beam detector at an accelerating voltage of 1.0 kV and a magnification
778 of ×12,000 (SU8240, Hitachi High Technologies).
779
780 **Data analysis**
781 The PPR was defined as the ratio of the amplitude of the second PSCs to the amplitude of the
782 first PSCs (100 ms inter-stimulus interval). The reduction in PSCs by a decrease in extracellular
783 Ca^{2+} concentration was determined by comparing 10 min baseline responses (2.5 mM Ca^{2+})
784 with responses 20–25 min after replacement of extracellular Ca^{2+} (1 mM). The inhibition of
785 PSCs by DCG-IV, baclofen, ω-CgTx, ω-Aga-IVA, BAPTA-AM, and EGTA-AM was
786 determined by comparing the 10 min baseline responses with responses at 15–20 min (or 25–30
787 min for BAPTA-AM, and EGTA-AM) after each drug application. The PSCs probability was
788 calculated as the percentage of the number of synaptic responses among 100 sweeps. Train
789 stimulation-induced depression was calculated as the ratio of the amplitude of the second to
790 10th PSCs to the amplitude of the first PSCs. Each stimulus point had an averaged of 10–20
791 sweeps. Spike probability was calculated as the percentage of the number of spikes among 10
792 trials.
793
794 **Statistics**
795 Statistical analyses were performed using OriginPro software (OriginLab, USA). Normality of
796 the distributions was assessed using the Shapiro–Wilk test. For samples with normal
797 distributions, Student's unpaired and paired two-tailed t tests were used to assess the between-
798 group and within-group differences, respectively. For samples that were not normally
799 distributed, a non-parametric paired sample Wilcoxon signed-rank test was used. The
800 Kolmogorov–Smirnov test was used for cumulative distributions. Differences among two or

multiple samples were assessed by using one-way or two-way ANOVA followed by Tukey's *post hoc* test for multiple comparisons. Statistical significance was set at $p < 0.05$ (***, **, and * indicates $p < 0.001$, $p < 0.01$ and $p < 0.05$, respectively). All values are reported as the mean ± SEM.

Acknowledgement

This work was supported by the Grants-in-Aid for Scientific Research (JP24KJ2139 to H. H.; JP20KK0171 and JP24K02125 to T.S.; JP20H03358, JP23H04240, and JP23K18167 to Y.H.) from Japan Society for the Promotion of Science (JSPS), the Takeda Science Foundation (to Y.H. and T.S.), the Naito Foundation (to Y.H.), the Mochida Memorial Foundation for Medical and Pharmaceutical Research (to Y.H.), JSPS Core-to-Core Program A. Advanced Research Networks (grant number: JPJSCCA20220007 to T.S.) and Grant-in-Aid for Transformative Research Areas—Platforms for Advanced Technologies and Research Resources "Advanced Bioimaging Support" (grant number: JP22H04926).

Author contributions

T.S. and Y.H. designed the experiments. H.H. and Y.H. performed the experiments and data analysis. K.K., M.Y. and M.W. designed and performed the immunohistochemistry experiments. Y.H. wrote the manuscript with input from all authors.

Declaration of interests

The authors declare no competing interests.

825 **References**

826

827 Adler EM, Augustine GJ, Duffy SN, Charlton MP (1991) Alien intracellular calcium chelators
828 attenuate neurotransmitter release at the squid giant synapse. J Neurosci 11:1496-1507.

829 Ajibola MI, Wu JW, Abdulmajeed WI, Lien CC (2021) Hypothalamic Glutamate/GABA
830 Cotransmission Modulates Hippocampal Circuits and Supports Long-Term
831 Potentiation. J Neurosci 41:8181-8196.

832 Alabi AA, Tsien RW (2012) Synaptic vesicle pools and dynamics. Cold Spring Harb Perspect
833 Biol 4:a013680.

834 Asmerian H, Alberts J, Sanetra AM, Diaz AJ, Silm K (2024) Role of adaptor protein complexes
835 in generating functionally distinct synaptic vesicle pools. J Physiol.

836 Billwiller F, Castillo L, Elseedy H, Ivanov AI, Scapula J, Ghestem A, Carponcy J, Libourel PA,
837 Bras H, Abdelmeguid NE, Krook-Magnuson E, Soltesz I, Bernard C, Luppi PH,
838 Esclapez M (2020) GABA-glutamate supramammillary neurons control theta and
839 gamma oscillations in the dentate gyrus during paradoxical (REM) sleep. Brain Struct
840 Funct 225:2643-2668.

841 Boulland JL, Jenstad M, Boekel AJ, Wouterlood FG, Edwards RH, Storm-Mathisen J,
842 Chaudhry FA (2009) Vesicular glutamate and GABA transporters sort to distinct sets of
843 vesicles in a population of presynaptic terminals. Cereb Cortex 19:241-248.

844 Brenowitz S, Trussell LO (2001) Minimizing synaptic depression by control of release
845 probability. J Neurosci 21:1857-1867.

846 Chamberland S, Toth K (2016) Functionally heterogeneous synaptic vesicle pools support
847 diverse synaptic signalling. J Physiol 594:825-835.

848 Chen S, He L, Huang AJY, Boehringer R, Robert V, Wintzer ME, Polygalov D, Weitemier AZ,
849 Tao Y, Gu M, Middleton SJ, Namiki K, Hama H, Therreau L, Chevaleyre V, Hioki H,
850 Miyawaki A, Piskorowski RA, McHugh TJ (2020) A hypothalamic novelty signal
851 modulates hippocampal memory. Nature 586:270-274.

852 Dugue GP, Dumoulin A, Triller A, Dieudonne S (2005) Target-dependent use of co-released
853 inhibitory transmitters at central synapses. J Neurosci 25:6490-6498.

854 Eccles JC, Fatt P, Koketsu K (1954) Cholinergic and inhibitory synapses in a pathway from
855 motor-axon collaterals to motoneurones. J Physiol 126:524-562.

856 Eggermann E, Bucurenciu I, Goswami SP, Jonas P (2011) Nanodomain coupling between
857 Ca(2)(+) channels and sensors of exocytosis at fast mammalian synapses. Nat Rev
858 Neurosci 13:7-21.

859 Farrell JS, Lovett-Barron M, Klein PM, Sparks FT, Gschwind T, Ortiz AL, Ahanonu B,
860 Bradbury S, Terada S, Oijala M, Hwaun E, Dudok B, Szabo G, Schnitzer MJ,
861 Deisseroth K, Losonczy A, Soltesz I (2021) Supramammillary regulation of locomotion
862 and hippocampal activity. Science 374:1492-1496.

863 Farsi Z, Preobraschenski J, van den Bogaart G, Riedel D, Jahn R, Woehler A (2016) Single-
864 vesicle imaging reveals different transport mechanisms between glutamatergic and
865 GABAergic vesicles. Science 351:981-984.

866 Fortin GM, Ducrot C, Giguere N, Kouwenhoven WM, Bourque MJ, Pacelli C, Varaschin RK,
867 Brill M, Singh S, Wiseman PW, Trudeau LE (2019) Segregation of dopamine and
868 glutamate release sites in dopamine neuron axons: regulation by striatal target cells.
869 FASEB J 33:400-417.

870 Foster KA, Regehr WG (2004) Variance-mean analysis in the presence of a rapid antagonist
871 indicates vesicle depletion underlies depression at the climbing fiber synapse. Neuron
872 43:119-131.

873 Frahm S, Antolin-Fontes B, Gorlich A, Zander JF, Ahnert-Hilger G, Ibanez-Tallon I (2015) An
874 essential role of acetylcholine-glutamate synergy at habenular synapses in nicotine
875 dependence. Elife 4:e11396.

876 Granger AJ, Wang W, Robertson K, El-Rifai M, Zanello AF, Bistrong K, Saunders A, Chow
877 BW, Nunez V, Turrero Garcia M, Harwell CC, Gu C, Sabatini BL (2020) Cortical
878 ChAT(+) neurons co-transmit acetylcholine and GABA in a target- and brain-region-
879 specific manner. Elife 9.

880 Hashimotodani Y, Karube F, Yanagawa Y, Fujiyama F, Kano M (2018) Supramammillary
881 Nucleus Afferents to the Dentate Gyrus Co-release Glutamate and GABA and
882 Potentiate Granule Cell Output. Cell Rep 25:2704-2715 e2704.

883 Hashimotodani Y, Nasrallah K, Jensen KR, Chavez AE, Carrera D, Castillo PE (2017) LTP at
884 Hilar Mossy Cell-Dentate Granule Cell Synapses Modulates Dentate Gyrus Output by
885 Increasing Excitation/Inhibition Balance. Neuron 95:928-943 e923.

886 Heine M, Groc L, Frischknecht R, Beique JC, Lounis B, Rumbaugh G, Huganir RL, Cognet L,
887 Choquet D (2008) Surface mobility of postsynaptic AMPARs tunes synaptic
888 transmission. Science 320:201-205.

889 Hirai H, Sakaba T, Hashimotodani Y (2022) Subcortical glutamatergic inputs exhibit a Hebbian
890 form of long-term potentiation in the dentate gyrus. Cell Rep 41:111871.

891 Hnasko TS, Edwards RH (2012) Neurotransmitter corelease: mechanism and physiological
892 role. Annu Rev Physiol 74:225-243.

893 Ichikawa R, Yamasaki M, Miyazaki T, Konno K, Hashimoto K, Tatsumi H, Inoue Y, Kano M,
894 Watanabe M (2011) Developmental switching of perisomatic innervation from
895 climbing fibers to basket cell fibers in cerebellar Purkinje cells. J Neurosci 31:16916-
896 16927.

897 Ito HT, Moser EI, Moser MB (2018) Supramammillary Nucleus Modulates Spike-Time
898 Coordination in the Prefrontal-Thalamo-Hippocampal Circuit during Navigation.
899 Neuron 99:576-587 e575.

900 Jackman SL, Beneduce BM, Drew IR, Regehr WG (2014) Achieving high-frequency optical
901 control of synaptic transmission. J Neurosci 34:7704-7714.

902 Jonas P, Bischofberger J, Sandkuhler J (1998) Corelease of two fast neurotransmitters at a
903 central synapse. Science 281:419-424.

904 Kamondi A, Acsady L, Wang XJ, Buzsaki G (1998) Theta oscillations in somata and dendrites
905 of hippocampal pyramidal cells in vivo: activity-dependent phase-precession of action
906 potentials. Hippocampus 8:244-261.

907 Kawamura Y, Fukaya M, Maejima T, Yoshida T, Miura E, Watanabe M, Ohno-Shosaku T, Kano
908 M (2006) The CB1 cannabinoid receptor is the major cannabinoid receptor at excitatory
909 presynaptic sites in the hippocampus and cerebellum. J Neurosci 26:2991-3001.

910 Kesner AJ, Mozaffarilegha M, Thirtamara Rajamani K, Arima Y, Harony-Nicolas H,
911 Hashimotodani Y, Ito HT, Song J, Ikemoto S (2023) Hypothalamic Supramammillary
912 Control of Cognition and Motivation. J Neurosci 43:7538-7546.

913 Kim S, Sabatini BL (2023) Analytical approaches to examine gamma-aminobutyric acid and
914 glutamate vesicular co-packaging. Frontiers in Synaptic Neuroscience 14.

915 Kim S, Wallace ML, El-Rifai M, Knudsen AR, Sabatini BL (2022) Co-packaging of opposing
916 neurotransmitters in individual synaptic vesicles in the central nervous system. Neuron
917 110:1371-1384 e1377.

918 Kirk IJ, McNaughton N (1991) Supramammillary cell firing and hippocampal rhythmical slow
919 activity. Neuroreport 2:723-725.

920 Kocsis B, Vertes RP (1994) Characterization of neurons of the supramammillary nucleus and
921 mammillary body that discharge rhythmically with the hippocampal theta rhythm in the
922 rat. J Neurosci 14:7040-7052.

923 Konno K, Yamasaki M, Miyazaki T, Watanabe M (2023) Glyoxal fixation: An approach to
924 solve immunohistochemical problem in neuroscience research. Sci Adv 9:eadf7084.

925 Lee S, Kim K, Zhou ZJ (2010) Role of ACh-GABA cotransmission in detecting image motion
926 and motion direction. Neuron 68:1159-1172.

927 Lee S, Zhang Y, Chen M, Zhou ZJ (2016) Segregated Glycine-Glutamate Co-transmission from
928 vGluT3 Amacrine Cells to Contrast-Suppressed and Contrast-Enhanced Retinal
929 Circuits. Neuron 90:27-34.

930 Li H, Santos MS, Park CK, Dobry Y, Voglmaier SM (2017) VGLUT2 Trafficking Is
931 Differentially Regulated by Adaptor Proteins AP-1 and AP-3. Front Cell Neurosci
932 11:324.

933 Li Y, Bao H, Luo Y, Yoan C, Sullivan HA, Quintanilla L, Wickersham I, Lazarus M, Shih YI,
934 Song J (2020) Supramammillary nucleus synchronizes with dentate gyrus to regulate
935 spatial memory retrieval through glutamate release. Elife 9.

936 Ma S, Hangya B, Leonard CS, Wisden W, Gundlach AL (2018) Dual-transmitter systems
937 regulating arousal, attention, learning and memory. Neurosci Biobehav Rev 85:21-33.

938 Magee JC (2001) Dendritic mechanisms of phase precession in hippocampal CA1 pyramidal
939 neurons. J Neurophysiol 86:528-532.

940 Markwardt SJ, Wadiche JI, Overstreet-Wadiche LS (2009) Input-specific GABAergic
941 signaling to newborn neurons in adult dentate gyrus. J Neurosci 29:15063-15072.

942 Miki T, Hashimotodani Y, Sakaba T (2022) Synaptic vesicle dynamics at the calyx of Held and
943 other central synapses. In: Exocytosis: From Molecules to Cells, pp 13-11-13-18: IOP
944 Publishing.

945 Miura E, Fukaya M, Sato T, Sugihara K, Asano M, Yoshioka K, Watanabe M (2006) Expression
946 and distribution of JNK/SAPK-associated scaffold protein JSAP1 in developing and
947 adult mouse brain. J Neurochem 97:1431-1446.

948 Miyazaki T, Fukaya M, Shimizu H, Watanabe M (2003) Subtype switching of vesicular
949 glutamate transporters at parallel fibre-Purkinje cell synapses in developing mouse
950 cerebellum. Eur J Neurosci 17:2563-2572.

951 Nabekura J, Katsurabayashi S, Kakazu Y, Shibata S, Matsubara A, Jinno S, Mizoguchi Y,
952 Sasaki A, Ishibashi H (2004) Developmental switch from GABA to glycine release in
953 single central synaptic terminals. Nat Neurosci 7:17-23.

954 Nakatsu F, Okada M, Mori F, Kumazawa N, Iwasa H, Zhu G, Kasagi Y, Kamiya H, Harada A,
955 Nishimura K, Takeuchi A, Miyazaki T, Watanabe M, Yuasa S, Manabe T, Wakabayashi
956 K, Kaneko S, Saito T, Ohno H (2004) Defective function of GABA-containing synaptic
957 vesicles in mice lacking the AP-3B clathrin adaptor. J Cell Biol 167:293-302.

958 Neher E, Brose N (2018) Dynamically Primed Synaptic Vesicle States: Key to Understand
959 Synaptic Short-Term Plasticity. Neuron 100:1283-1291.

960 Ntamati NR, Luscher C (2016) VTA Projection Neurons Releasing GABA and Glutamate in
961 the Dentate Gyrus. eNeuro 3.

962 Nusbaum MP, Blitz DM, Swensen AM, Wood D, Marder E (2001) The roles of co-transmission
963 in neural network modulation. Trends Neurosci 24:146-154.

964 Paxinos G, Franklin KBJ (2001) The mouse brain in stereotaxic coordinates, 2nd Edition. San
965 Diego: Academic Press.

966 Pedersen NP, Ferrari L, Venner A, Wang JL, Abbott SBG, Vujovic N, Arrigoni E, Saper CB,
967 Fuller PM (2017) Supramammillary glutamate neurons are a key node of the arousal
968 system. Nat Commun 8:1405.

969 Ren J, Qin C, Hu F, Tan J, Qiu L, Zhao S, Feng G, Luo M (2011) Habenula "cholinergic"
970 neurons co-release glutamate and acetylcholine and activate postsynaptic neurons via
971 distinct transmission modes. Neuron 69:445-452.

972 Robert V, Therreau L, Chevaleyre V, Lepicard E, Viollet C, Cognet J, Huang AJ, Boehringer
973 R, Polygalov D, McHugh TJ, Piskorowski RA (2021) Local circuit allowing
974 hypothalamic control of hippocampal area CA2 activity and consequences for CA1.
975 Elife 10.

976 Root DH, Mejias-Aponte CA, Zhang S, Wang HL, Hoffman AF, Lupica CR, Morales M (2014)
977 Single rodent mesohabenular axons release glutamate and GABA. Nat Neurosci
978 17:1543-1551.

979 Root DH, Zhang S, Barker DJ, Miranda-Barrientos J, Liu B, Wang HL, Morales M (2018)
980 Selective Brain Distribution and Distinctive Synaptic Architecture of Dual
981 Glutamatergic-GABAergic Neurons. Cell Rep 23:3465-3479.

982 Rost BR, Wietek J, Yizhar O, Schmitz D (2022) Optogenetics at the presynapse. Nat Neurosci
983 25:984-998.

984 Sakaba T (2008) Two Ca(2+)-dependent steps controlling synaptic vesicle fusion and
985 replenishment at the cerebellar basket cell terminal. Neuron 57:406-419.

986 Santos MS, Park CK, Foss SM, Li H, Voglmaier SM (2013) Sorting of the vesicular GABA
987 transporter to functional vesicle pools by an atypical dileucine-like motif. J Neurosci
988 33:10634-10646.

989 Saunders A, Oldenburg IA, Berezovskii VK, Johnson CA, Kingery ND, Elliott HL, Xie T,
990 Gerfen CR, Sabatini BL (2015) A direct GABAergic output from the basal ganglia to
991 frontal cortex. Nature 521:85-89.

992 Schmidt-Hieber C, Jonas P, Bischofberger J (2004) Enhanced synaptic plasticity in newly
993 generated granule cells of the adult hippocampus. Nature 429:184-187.

994 Sengupta A, Bocchio M, Bannerman DM, Sharp T, Capogna M (2017) Control of Amygdala
995 Circuits by 5-HT Neurons via 5-HT and Glutamate Cotransmission. J Neurosci
996 37:1785-1796.

997 Shabel SJ, Proulx CD, Piriz J, Malinow R (2014) Mood regulation. GABA/glutamate co-
998 release controls habenula output and is modified by antidepressant treatment. Science
999 345:1494-1498.

1000 Silm K, Yang J, Marcott PF, Asensio CS, Eriksen J, Guthrie DA, Newman AH, Ford CP,
1001 Edwards RH (2019) Synaptic Vesicle Recycling Pathway Determines Neurotransmitter
1002 Content and Release Properties. Neuron 102:786-800 e785.

1003 Soussi R, Zhang N, Tahtakran S, Houser CR, Esclapez M (2010) Heterogeneity of the
1004 supramammillary-hippocampal pathways: evidence for a unique GABAergic
1005 neurotransmitter phenotype and regional differences. Eur J Neurosci 32:771-785.

1006 Sudhof TC (2013) Neurotransmitter release: the last millisecond in the life of a synaptic vesicle.
1007 Neuron 80:675-690.

1008 Tabuchi E, Sakaba T, Hashimotodani Y (2022) Excitatory selective LTP of supramammillary
1009 glutamatergic/GABAergic cotransmission potentiates dentate granule cell firing. Proc
1010 Natl Acad Sci U S A 119:e2119636119.

1011 Takacs VT, Cserep C, Schlingloff D, Posfai B, Szonyi A, Sos KE, Kornyei Z, Denes A, Gulyas
1012 AI, Freund TF, Nyiri G (2018) Co-transmission of acetylcholine and GABA regulates
1013 hippocampal states. Nat Commun 9:2848.

1014 Takamori S et al. (2006) Molecular anatomy of a trafficking organelle. Cell 127:831-846.

1015 Takasaki C, Yamasaki M, Uchigashima M, Konno K, Yanagawa Y, Watanabe M (2010)
1016 Cytochemical and cytological properties of perineuronal oligodendrocytes in the mouse
1017 cortex. Eur J Neurosci 32:1326-1336.

1018 Tritsch NX, Granger AJ, Sabatini BL (2016) Mechanisms and functions of GABA co-release.
1019 Nat Rev Neurosci 17:139-145.

1020 Trudeau LE, El Mestikawy S (2018) Glutamate Cotransmission in Cholinergic, GABAergic
1021 and Monoamine Systems: Contrasts and Commonalities. Front Neural Circuits 12:113.

1022 Trudeau LE, Hnasko TS, Wallen-Mackenzie A, Morales M, Rayport S, Sulzer D (2014) The
1023 multilingual nature of dopamine neurons. Prog Brain Res 211:141-164.

1024 Trussell LO, Zhang S, Raman IM (1993) Desensitization of AMPA receptors upon multiquantal
1025 neurotransmitter release. Neuron 10:1185-1196.

1026 Turecek J, Jackman SL, Regehr WG (2016) Synaptic Specializations Support Frequency-
1027 Independent Purkinje Cell Output from the Cerebellar Cortex. Cell Rep 17:3256-3268.

1028 Uchigashima M, Yamazaki M, Yamasaki M, Tanimura A, Sakimura K, Kano M, Watanabe M
1029 (2011) Molecular and morphological configuration for 2-arachidonoylglycerol-
1030 mediated retrograde signaling at mossy cell-granule cell synapses in the dentate gyrus.
1031 J Neurosci 31:7700-7714.

1032 Vaaga CE, Borisovska M, Westbrook GL (2014) Dual-transmitter neurons: functional
1033 implications of co-release and co-transmission. Curr Opin Neurobiol 29:25-32.

1034 Voglmaier SM, Kam K, Yang H, Fortin DL, Hua Z, Nicoll RA, Edwards RH (2006) Distinct
1035 endocytic pathways control the rate and extent of synaptic vesicle protein recycling.
1036 Neuron 51:71-84.

1037 Wadiche JI, Jahr CE (2001) Multivesicular release at climbing fiber-Purkinje cell synapses.
1038 Neuron 32:301-313.

1039 Wallace ML, Sabatini BL (2023) Synaptic and circuit functions of multitransmitter neurons in
1040 the mammalian brain. Neuron 111:2969-2983.

1041 Wallace ML, Saunders A, Huang KW, Philson AC, Goldman M, Macosko EZ, McCarroll SA,
1042 Sabatini BL (2017) Genetically Distinct Parallel Pathways in the Entopeduncular
1043 Nucleus for Limbic and Sensorimotor Output of the Basal Ganglia. Neuron 94:138-152
1044 e135.

1045 Weston MC, Nehring RB, Wojcik SM, Rosenmund C (2011) Interplay between VGLUT
1046 isoforms and endophilin A1 regulates neurotransmitter release and short-term plasticity.
1047 Neuron 69:1147-1159.

1048 Wong AY, Graham BP, Billups B, Forsythe ID (2003) Distinguishing between presynaptic and
1049 postsynaptic mechanisms of short-term depression during action potential trains. J
1050 Neurosci 23:4868-4877.

1051 Wu LG, Saggau P (1994) Pharmacological identification of two types of presynaptic voltage-
1052 dependent calcium channels at CA3-CA1 synapses of the hippocampus. J Neurosci
1053 14:5613-5622.

1054 Yoo JH, Zell V, Gutierrez-Reed N, Wu J, Ressler R, Shenasa MA, Johnson AB, Fife KH, Faget
1055 L, Hnasko TS (2016) Ventral tegmental area glutamate neurons co-release GABA and
1056 promote positive reinforcement. Nat Commun 7:13697.

1057 Zhang S, Qi J, Li X, Wang HL, Britt JP, Hoffman AF, Bonci A, Lupica CR, Morales M (2015)
1058 Dopaminergic and glutamatergic microdomains in a subset of rodent mesoaccumbens
1059 axons. Nat Neurosci 18:386-392.

1060 Zucker RS, Regehr WG (2002) Short-term synaptic plasticity. Annu Rev Physiol 64:355-405.

1061 Zych SM, Ford CP (2022) Divergent properties and independent regulation of striatal
1062 dopamine and GABA co-transmission. Cell Rep 39:110823.
1063
1064

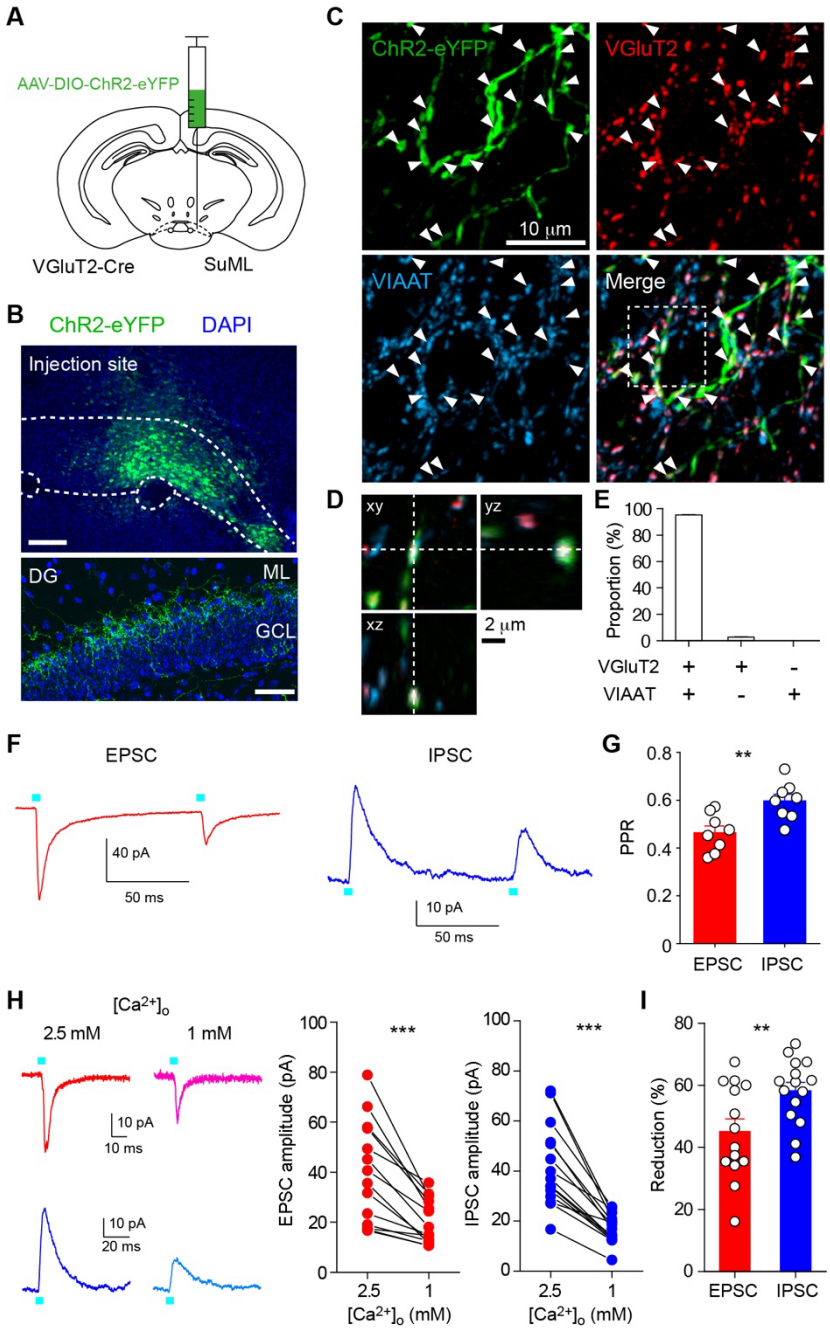

Figure 1. Different PPRs and Ca^{2+} sensitivities of glutamate/GABA co-transmission at SuM-GC synapses

(**A**) Diagram illustrating the injection of AAV-DIO-ChR2(H134R)-eYFP into the lateral part of SuM of VGluT2-Cre mouse. (**B**) (top) Fluorescence image showing the injection site of AAV in the SuM. (bottom) ChR2(H134R)-eYFP-expressing SuM axons are observed in the supragranular layer of the DG. ML, molecular layer; GCL, granule cell layer. Scale bars, Top, 200 μm; Bottom, 50 μm. (**C**) Z-stacked immunofluorescence images double stained for VGluT2 (red) and VIAAT (cyan). The merged image demonstrates the colocalization of VGluT2 and VIAAT in the ChR2-eYFP-expressing SuM terminals (arrowheads). (**D**) Higher

magnification xy, xz, and yz projection images outlined in boxed area in (C) show that a SuM bouton is co-stained with VGluT2 and VIAAT. (**E**) Proportion of VGluT2- and/or VIAAT-expressing boutons in the ChR2-eYFP labeled boutons (2205 boutons, 7 slices). Both VGluT2 and VIAAT (95.2 ± 0.3%), VGluT2 only (2.7 ± 0.2%), and VIAAT only (0%). (**F**) Representative traces of EPSC (red, V_h = –70 mV) and IPSC (blue, V_h = 0 mV) evoked with paired pulse illumination (100 ms interval). (**G**) Summary plot of PPR showing a significant difference between EPSC and IPSC. (**H**) Representative traces (left) and summary plots (right) of EPSCs and IPSCs in 2.5 and 1 mM extracellular Ca^{2+}. (**I**) Summary plot of percent reduction in the amplitudes of EPSCs and IPSCs from 2.5 to 1 mM extracellular Ca^{2+}. Data are presented as mean ± SEM. **$p < 0.01$, ***$p < 0.001$.

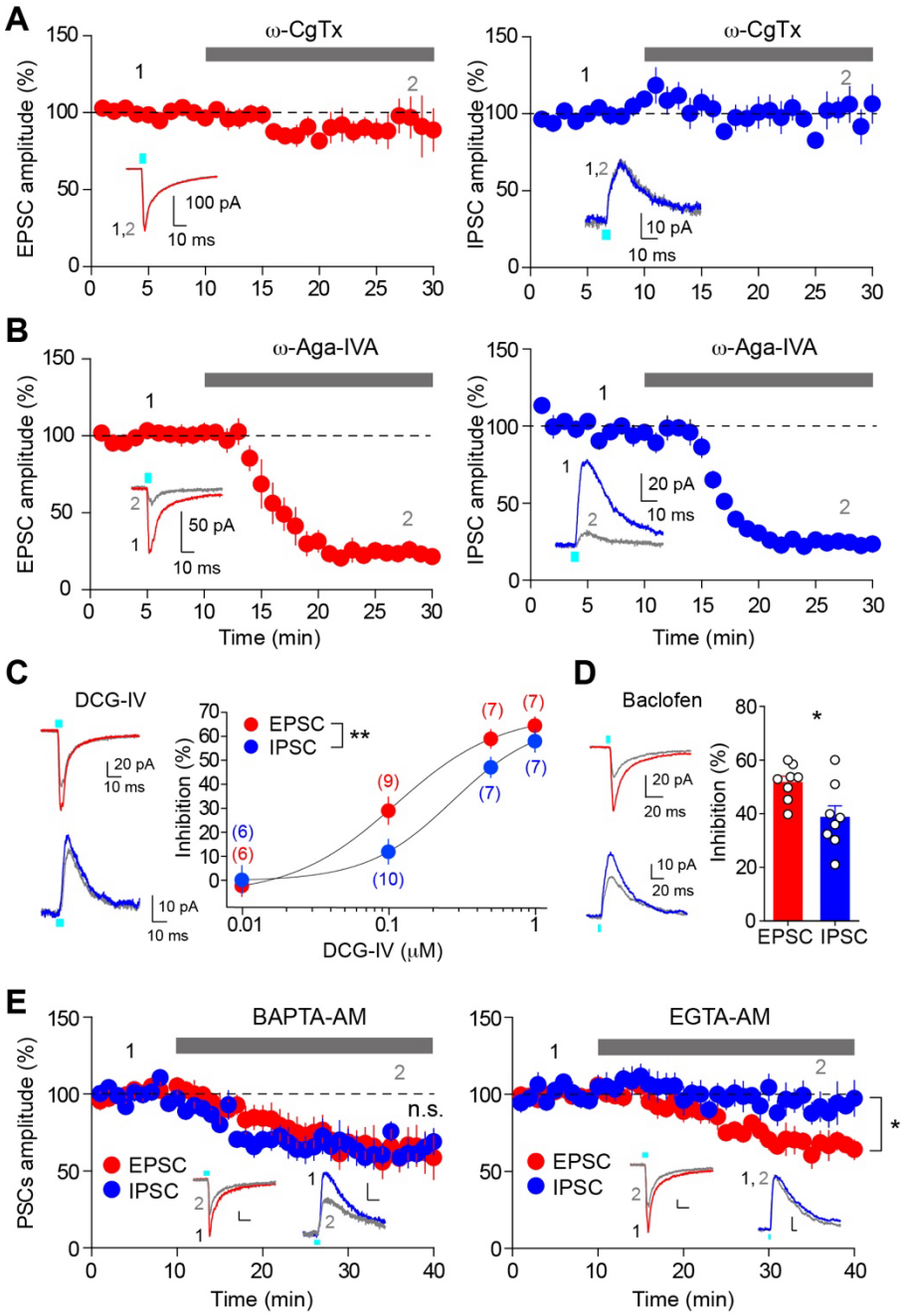

Figure 2. Different presynaptic modulation and Ca^{2+} chelator-sensitivities of glutamate/GABA co-transmission

(**A**) Time course summary plots showing the effects of ω-CgTx (500 nM) on co-transmission of glutamate (left) and GABA (right) at SuM-GC synapses. Insets indicate representative traces. (**B**) Time course summary plots showing that the co-transmission of glutamate (left) and GABA (right) at SuM-GC synapses were inhibited by ω-Aga-IVA (200 nM). Insets show representative traces. (**C**) (left) Representative traces before (EPSC, red; IPSC, blue) and after (gray) application of DCG-IV (0.1 μM). (right) Summary plot of concentration-response curves. Data are fitted to the Hill equation. Numbers in parentheses indicate the number of

1153 cells. (**D**) (left) Representative traces before (EPSC, red; IPSC, blue) and after (gray)
1154 application of baclofen (5 μM). (right) Summary plot of percent inhibition in the amplitudes
1155 of EPSCs and IPSCs by 5 μM baclofen. (**E**) Time course summary plots showing the sensitivity
1156 of EPSCs and IPSCs to 100 μM BAPTA-AM (left) and 100 μM EGTA-AM (right). Insets show
1157 representative traces. Calibration: 10 pA, 10 ms. Data are presented as mean ± SEM. *$p < 0.05$,
1158 **$p < 0.01$. n.s., not significant.
1159

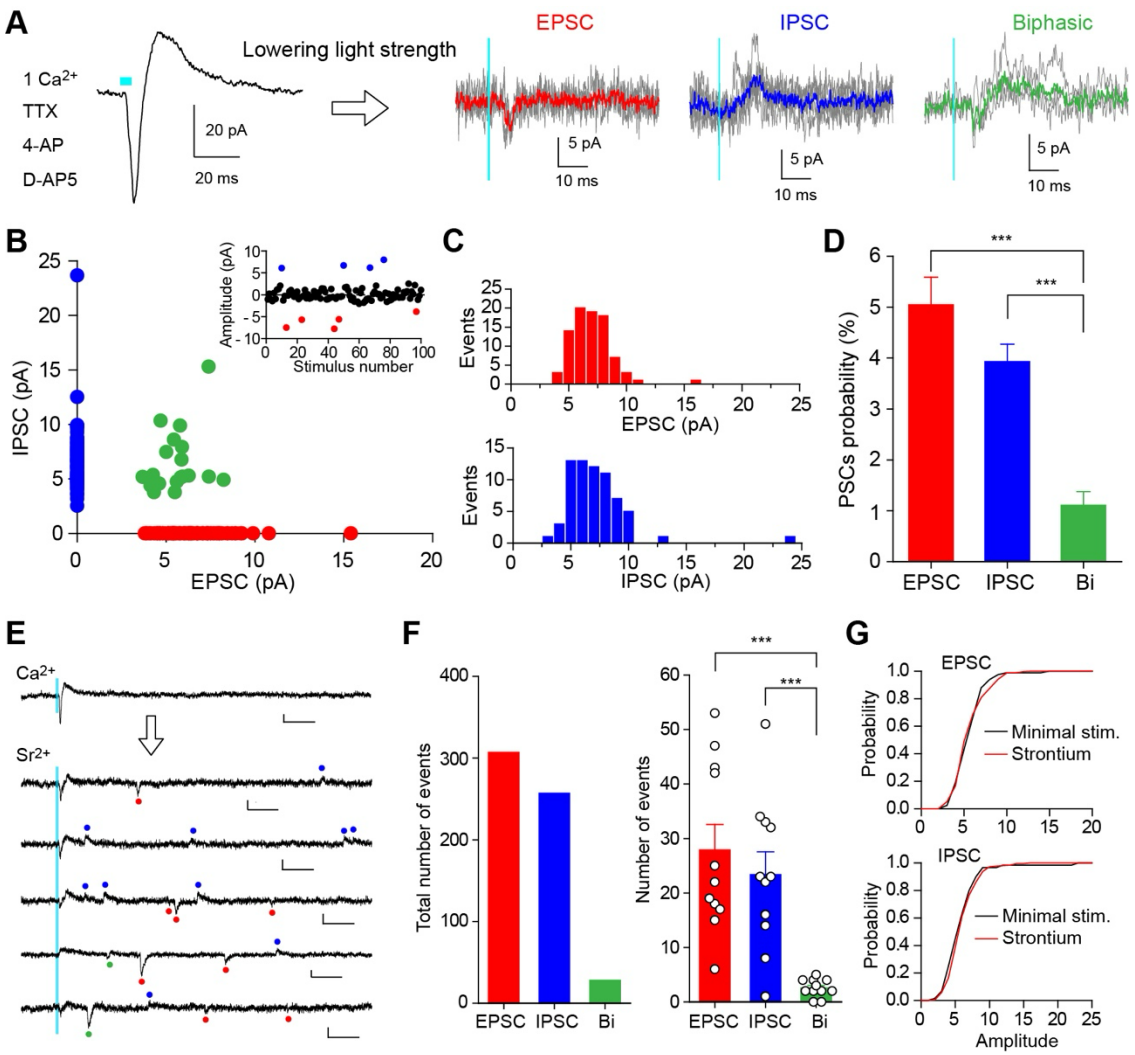

Figure 3. Uniquantal release-mediated synaptic responses evoked by minimal light stimulation or strontium-induced asynchronous release at SuM-GC synapses

(**A**) Representative traces of biphasic response elicited by light stimulation with maximum light power (left) and stochastically evoked PSCs with minimal light stimulation (100 trials for each cell) (right). Synaptic responses at SuM-GC synapses were recorded at holding potentials of –20 to –30 mV in the presence of TTX (1 μM), 4-AP (1 mM), D-AP5 (50 μM), and Ca^{2+} (1 mM). Average EPSC (red), IPSC (blue), and biphasic current (green) are superimposed on individual traces. (**B**) Scatter plot of the amplitude of IPSCs against the amplitude of EPSCs recorded from 17 cells. Success events of 172 PSCs are plotted. (Inset) A single experiment showing 100 trials with an interval of 10 sec elicited stochastically EPSCs (red) and IPSCs (blue). (**C**) Amplitude histograms of EPSCs (top) and IPSCs (bottom) in same data as in B. (**D**) Summary graph of PSCs probability. (**E**) Representative traces showing strontium-induced asynchronous release recorded from GC at holding potentials of –20 to –30 mV. The NMDA receptor antagonist D-AP5 (50 μM) was included in the extracellular solution to eliminate NMDA receptor-mediated EPSCs. Red, blue, and green points indicate detected EPSCs, IPSCs,

and biphasic currents, respectively. Calibration: 10 pA, 50 ms. (**F**) (left) Summary bar graph showing the total number of asynchronous quantal responses (n = 11, 30 trials for each cell) (EPSC: 307 events; IPSC: 257 events; biphasic: 28 events). (right) Averaged number of asynchronous events showing that the majority of asynchronous events are EPSCs and IPSCs, and a few biphasic responses. (**G**) Cumulative distributions of the amplitudes of EPSCs (top) and IPSCs (bottom) for minimal light stimulation-evoked PSCs and strontium-induced PSCs (EPSC: minimal stim.: 86 events from 17 cells; strontium: 307 events from 11 cells, $p = 0.72$; IPSC: minimal stim.: 67 events from 17 cells; strontium: 256 events from 11 cells, $p = 0.096$, Kolmogorov-Smirnov test). Data are presented as mean ± SEM. ***$p < 0.001$.

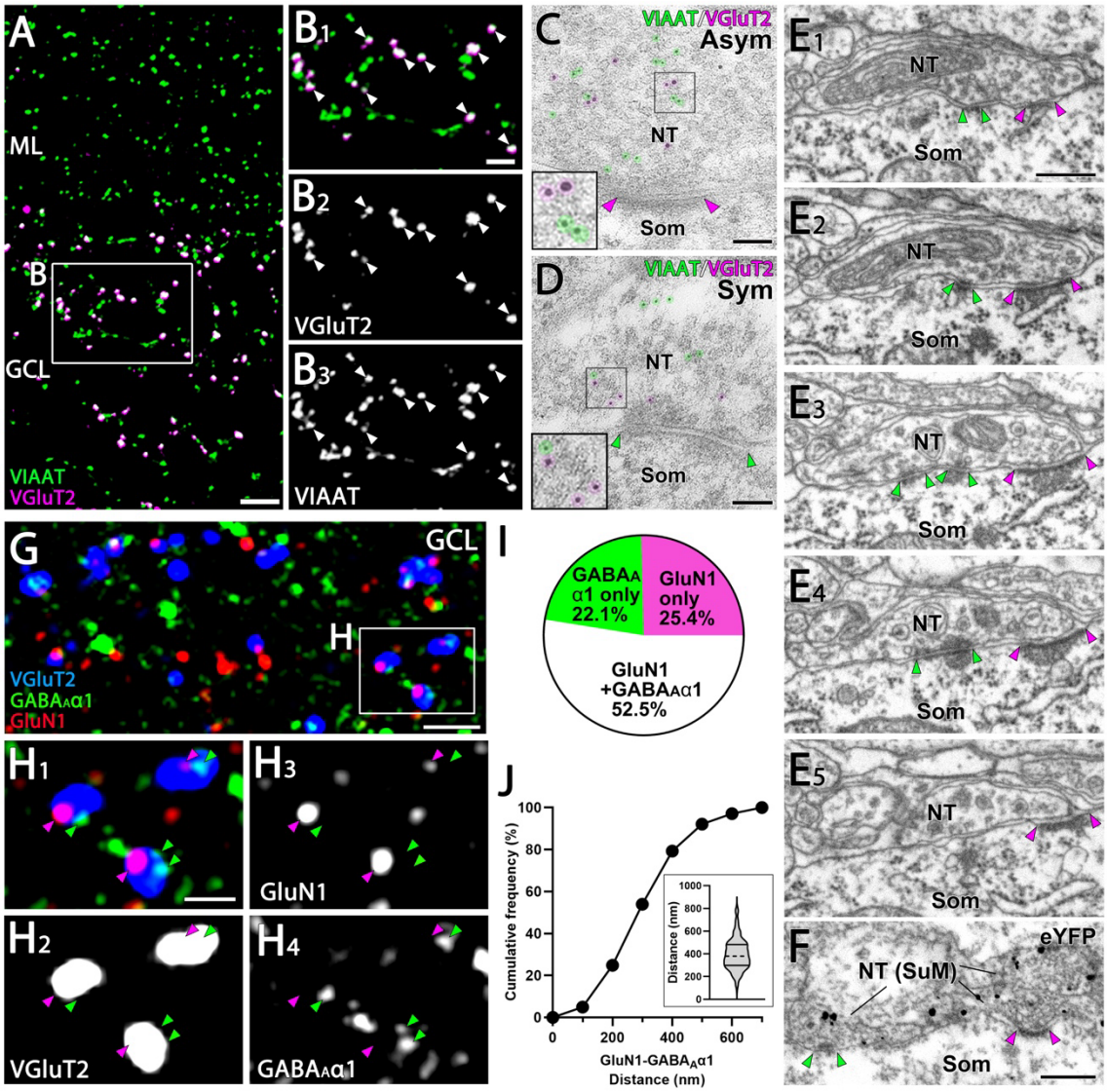

Figure 4. Close association of GluN1 and GABA$_A$α1 facing the identical SuM terminals (**A, B**) Double immunofluorescence for VIAAT (green) and VGluT2 (magenta) in the GC layer of the DG. (B) Higher magnification images of the boxed area in (A) show that VGluT2-positive terminals are consistently co-labeled with VIAAT (white arrowheads). (**C, D**) Post-embedding immunogold EM shows immunogold particles for VIAAT (green, 5 nm) and VGluT2 (magenta, 10 nm) colocalizing within the same terminal, forming asymmetric (C) and symmetric (D) synapses. NT, nerve terminal; Som, soma. (**E**) Five consecutive EM images depict a single NT forming both asymmetric and symmetric synapses with a GC soma. The postsynaptic densities of the asymmetric and symmetric synapses are indicated by magenta and green arrowheads, respectively. (**F**) A pre-embedding immunogold EM image demonstrates a single NT from SuM, labeled with eYFP, forming both asymmetric and symmetric synapses with a GC soma. The postsynaptic densities are similarly marked by magenta and green

1200 arrowheads. (**G, H**) Triple immunofluorescence for GluN1 (red), $GABA_A\alpha1$ (green), and
1201 VGluT2 (blue) in the GC layer of the DG. (**H**) Higher magnification of the boxed region in
1202 (G). Magenta arrowheads indicate GluN1 and green arrowheads indicate $GABA_A\alpha1$, both
1203 apposed to VGluT2 puncta. (**I**) The proportion of VGluT2-positive terminals in the GC layer
1204 associated with GluN1 *and/or* $GABA_A\alpha1$ immunoreactivity. Data are based on measurements
1205 from 634 VGluT2-positive terminals from two mice. (**J**) Cumulative distribution of the
1206 distance between GluN1 and $GABA_A\alpha1$ puncta associated with VGluT2-positive terminals in
1207 the GC layer that are double-labeled for GluN1 and $GABA_A\alpha1$. Data are based on
1208 measurements from 241 VGluT2-positive terminals from two mice (violin plot shown in the
1209 inset). The dashed line within each violin plot represents the median, while the solid lines at
1210 the top and bottom indicate the 75th and 25th percentiles, respectively. Scale bars: A, 5 μm; B,
1211 2 μm; C, D, 100 nm; E, F, 400 nm; G, 5 μm; H, 1 μm.
1212

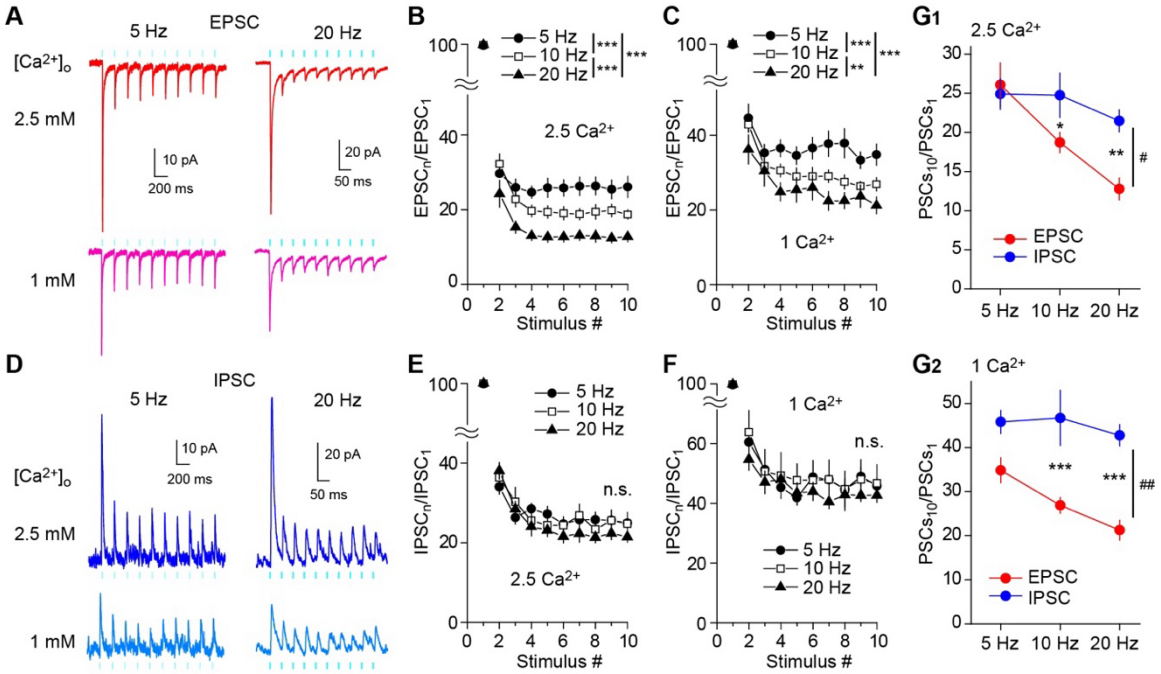

Figure 5. Frequency-dependent shift of glutamate/GABA co-transmission balance of SuM inputs in GCs

(**A, D**) Representative traces of EPSCs (V_h = –70 mV) (A) and IPSCs (V_h = 0 mV) (D) in response to 10 light stimuli at 5 Hz (left) or 20 Hz (right) in 2.5 mM (top) or 1 mM (bottom) extracellular Ca^{2+}. (**B**) Summary graph of normalized EPSC amplitude plotted against the stimulus number in 2.5 mM extracellular Ca^{2+}. Two-way repeated measures ANOVA, $F_{(2,16)}$ = 13.0, $p < 0.001$, n = 9 or 10; Tukey post hoc test: ***$p < 0.001$. (**C**) Same as (B), but recorded in 1 mM extracellular Ca^{2+}. Two-way repeated measures ANOVA, $F_{(2,16)}$ = 11.4, $p < 0.001$, n = 9 or 10; Tukey post hoc test: **$p < 0.01$, ***$p < 0.001$. (**E**) Summary graph of normalized IPSC amplitude plotted against stimulus number in 2.5 mM extracellular Ca^{2+}. Two-way repeated measures ANOVA, $F_{(2,16)}$ = 0.003, p = 0.997, n = 9. (**F**) Same as (E), but recorded in 1 mM extracellular Ca^{2+}. Two-way repeated measures ANOVA, $F_{(2,16)}$ = 0.02, p = 0.981, n = 9. (**G**) Summary plots showing the normalized amplitudes of 10th EPSCs and IPSCs at 5 Hz, 10 Hz, and 20 Hz in 2.5 mM extracellular Ca^{2+} (G1: two-way repeated measures ANOVA, $F_{(1,7)}$ = 8.03, $^{\#}p < 0.05$, n = 9 or 10; Tukey's post hoc test, EPSC versus IPSC, *$p < 0.05$, **$p < 0.01$), or in 1 mM extracellular Ca^{2+} (G2: two-way repeated measures ANOVA, $F_{(1,7)}$ = 21.76, $^{\#\#}p < 0.01$, n = 9 or 10; Tukey's post hoc test, EPSC versus IPSC, ***$p < 0.001$). n.s., not significant. Data are presented as mean ± SEM.

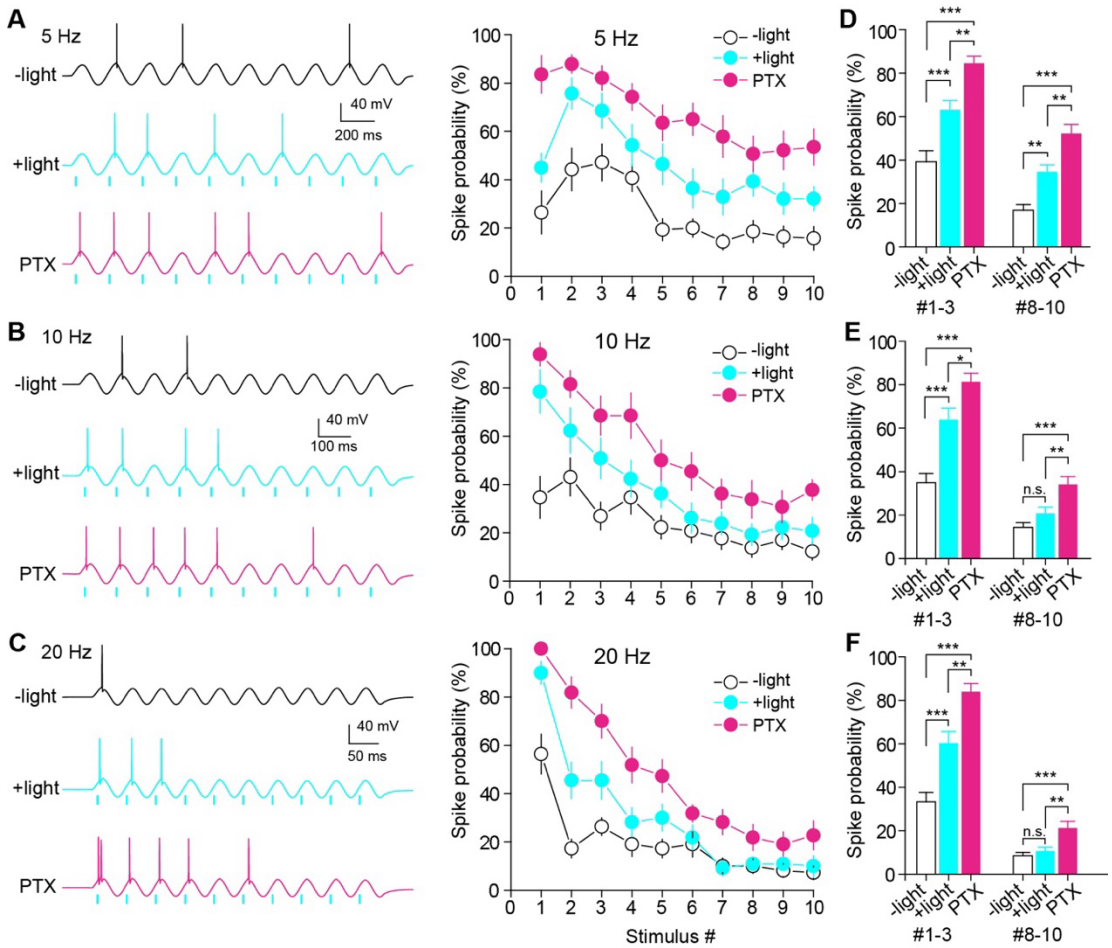

Figure 6. Frequency-dependent modulation of GC firing by SuM inputs

(**A-C**) (left) Representative traces showing GC spikes in response to sinusoidal current injections without (top) and with (middle) paired light stimulation of SuM inputs at 5 Hz (A), 10 Hz (B), and 20 Hz (C). Bottom trace showing the GC response to sinusoidal current injection paired with light stimulation in the presence of 100 μM picrotoxin (PTX). (right) Summary graph of spike probability against stimulus number. (**D-F**) Summary plots of spike probability at initial and last three stimulus numbers at 5 Hz (D), 10 Hz (E), and 20 Hz (F). The spike probabilities of stimulus numbers 1-3 and 8-10 were averaged. (D) one-way ANOVA, n = 14, $F_{(2,123)} = 28.8$, $p < 0.001$ (#1-3), $F_{(2,123)} = 25.8$, $p < 0.001$ (#8-10); Tukey's post hoc test, ***p < 0. 001, **p < 0. 01. (E) one-way ANOVA, n = 13, $F_{(2,114)} = 26.3$, $p < 0.001$ (#1-3), $F_{(2,114)} = 11.8$, $p < 0.001$ (#8-10); Tukey's post hoc test, ***p < 0. 001, **p < 0. 01, *p < 0.05, n.s., not significant. (F) one-way ANOVA, n = 11, $F_{(2,96)} = 31.4$, $p < 0.001$ (#1-3), $F_{(2,96)} = 9.2$, $p < 0.001$ (#8-10); Tukey's post hoc test, ***p < 0. 001, **p < 0.01, n.s., not significant. Data are presented as mean ± SEM.

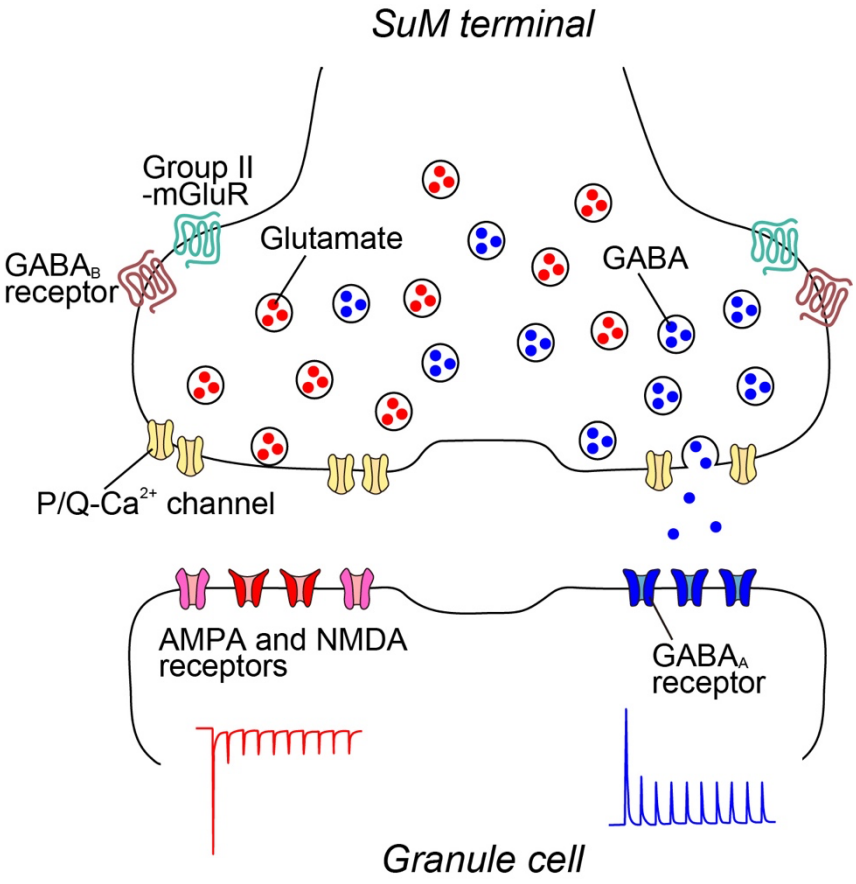

Figure 7. Working hypothesis of synaptic architecture of SuM-GC synapse

A single SuM terminal contains distinct glutamatergic and GABAergic vesicles, which are regulated by P/Q-type Ca^{2+} channels and also modulated by group II mGluRs and $GABA_B$ receptors. Glutamatergic and GABAergic vesicles are loosely and tightly coupled with Ca^{2+} channels, respectively. At the postsynaptic site of GCs, AMPA/NMDA and $GABA_A$ receptors are distributed separately. Based on their molecular composition, glutamatergic and GABAergic synapses are established independently, achieving the distinct glutamatergic and GABAergic transmission.

Supplementary Figures

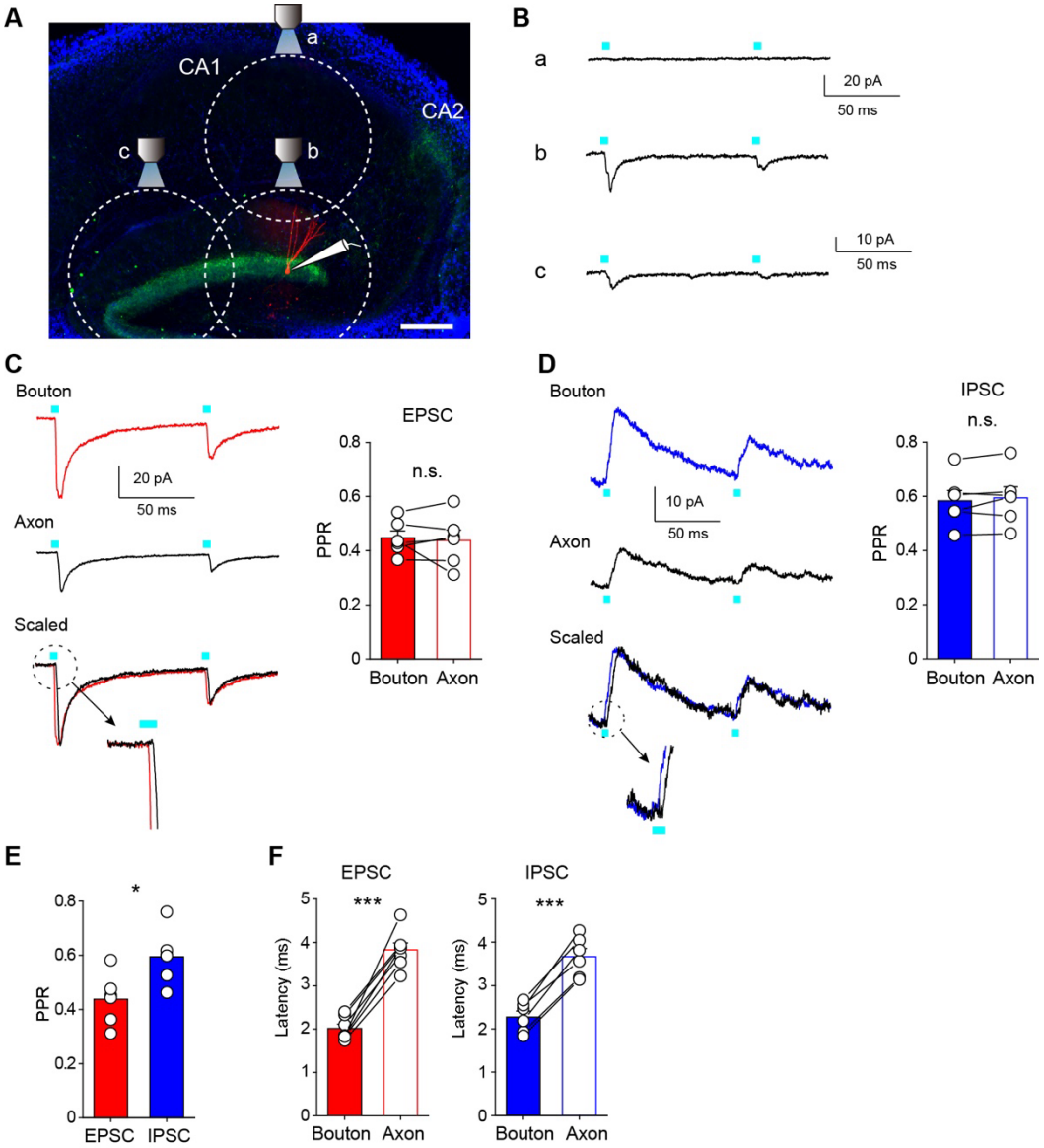

Figure 1-figure supplement 1. PPRs of glutamatergic and GABAergic co-transmission show no difference between over-axon and over-bouton illumination

(A) Diagram of the experimental setup. Fluorescence image of hippocampal slice shows ChR2-eYFP expressing SuM fibers (green) and a biocytin-filled GC (red). The dotted circles indicate the estimated LED illumination area at each location. We recorded from GCs located in the most edge of upper blade of GC layer (~150 μm). Once synaptic responses were observed by over-bouton illumination (over-the recorded cell soma, position b), then the objective lens was moved to ~600 μm vertically away in the stratum radiatum of the CA1 region (position a). The light power was adjusted to evoke no response at position a, indicating that SuM-GC synapses on the recorded GCs were out of the illumination field. The objective lens was then returned to position b, and PSCs of SuM-GC synapses were recorded with paired stimulation. Then, the

objective lens was moved ~600 μm along the GC layer (position c) to achieve over-axon illumination. Scale bar: 200 μm. **(B)** Representative traces of SuM-GC EPSCs evoked with over-CA1 (a), over-bouton (b), and over-axon (c) illumination. **(C, D)** Representative traces (left) and summary plots of PPRs (right) of SuM-GC EPSCs (C) or IPSCs (D) indicating no significant difference between over-bouton and over-axon illumination of SuM inputs (EPSC: bouton: 0.45 ± 0.03; axon: 0.44 ± 0.04, $n = 6$, $p = 0.72$, paired t-test; IPSC: bouton: 0.58 ± 0.04; axon: 0.59 ± 0.04, $n = 6$, $p = 0.32$, paired t-test). EPSCs or IPSCs were recorded with over-bouton (top) or over-axon (middle) illumination, respectively. Bottom traces show that a trace by over-axon stimulation was scaled to the peak of a trace by over-bouton stimulation. Magnified traces of the dotted circle show a delayed onset latency of a trace by over-axon stimulation relative to a trace by over-bouton stimulation. **(E)** Summary plot of PPR indicating a significant difference between EPSC and IPSC evoked by over-axon illumination (EPSC: 0.44 ± 0.04; IPSC: 0.59 ± 0.04, $n = 6$, $p < 0.05$, unpaired t-test). **(F)** Summary plots of latency to the onset of the synaptic response. The delayed latency of the synaptic responses by over-axon illumination indicates that synaptic transmission was mediated by light-evoked action potential propagation toward SuM terminals (EPSC: bouton: 2.0 ± 0.1 ms; axon: 3.8 ± 0.2 ms, $n = 7$, $p < 0.001$, paired t-test; IPSC: bouton: 2.3 ± 0.1 ms; axon: 3.7 ± 0.2 ms, $n = 6$, $p < 0.001$, paired t-test). Data are presented as mean ± SEM. *$p < 0.05$, ***$p < 0.001$, n.s., not significant.

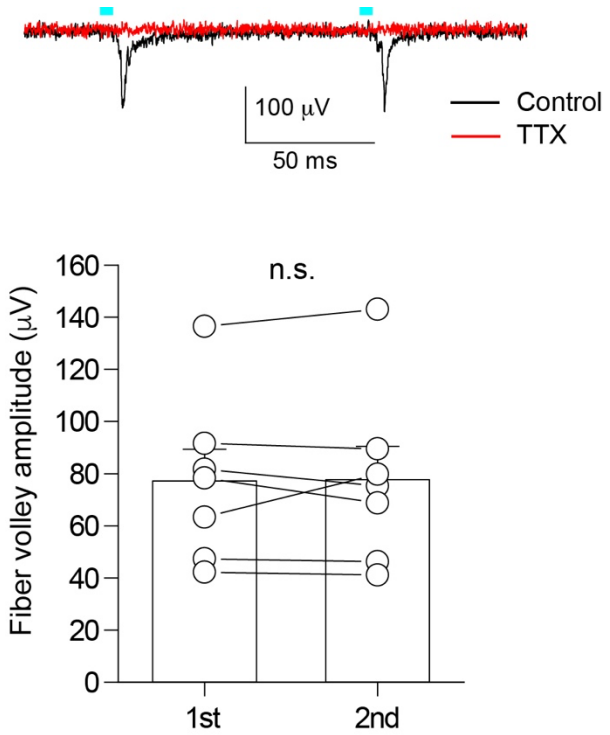

Figure 1-figure supplement 2. Paired-pulse light stimulation evoked similar amplitude of fiber volley

(top) Representative traces of the extracellularly recorded fiber volley from supragranular layer in response to paired light stimulation with 100 ms interval. 1 μM TTX completely blocked the fiber volley (red). To clearly isolate the fiber volley, light-evoked synaptic responses were blocked by 10 μM NBQX, 50 μM D-AP5, and 100 μM picrotoxin. (bottom) Summary plot of the fiber volley amplitude (n = 7, p = 0.91, paired t-test). Data are presented as mean ± SEM. n.s., not significant.

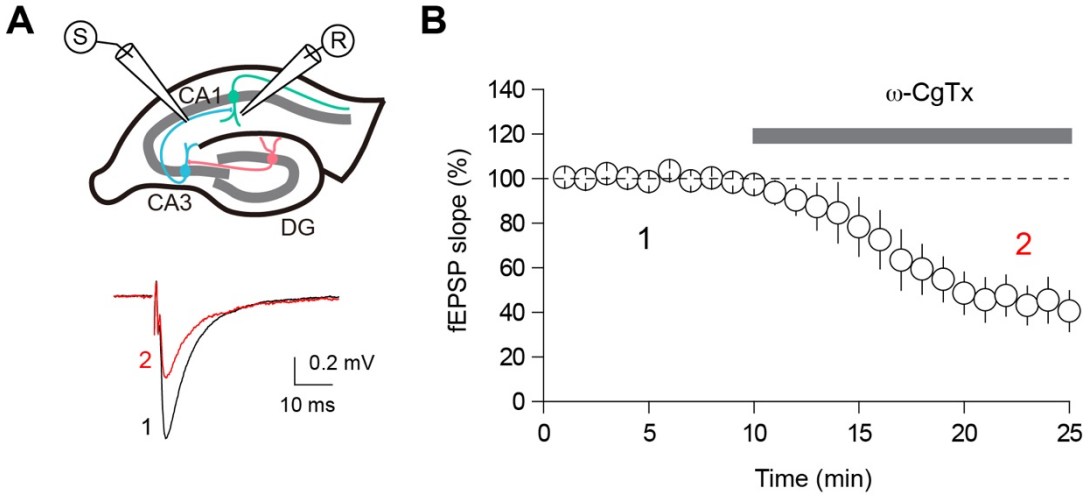

Figure 2-figure supplement 1. The effect of ω-CgTx on CA3-CA1 transmission
(**A**) (top) Schematic diagram illustrating the extracellular field excitatory postsynaptic potential recording (fEPSP) configuration. Both the recording and stimulating electrodes were placed in the stratum radiatum of CA1. (bottom) Representative fEPSP traces before (black) and after (red) application of ω-CgTx (500 nM). (**B**) Summary time course plot showing inhibition of CA3-CA1 transmission by ω-CgTx (44.5 ± 9.5% of baseline, n = 5, $p < 0.01$, paired t-test). Data are presented as mean ± SEM.

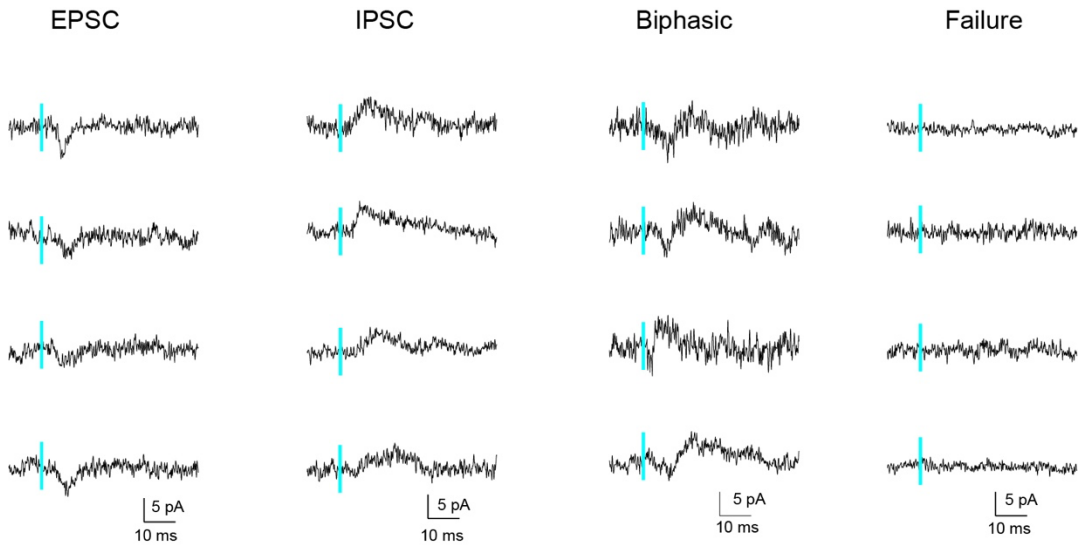

Figure 3-figure supplement 1. Minimal light stimulation-evoked synaptic responses at SuM-GC synapses

Sample traces recorded from GCs at holding potential of –20 to –30 mV in response to minimal light stimulation.

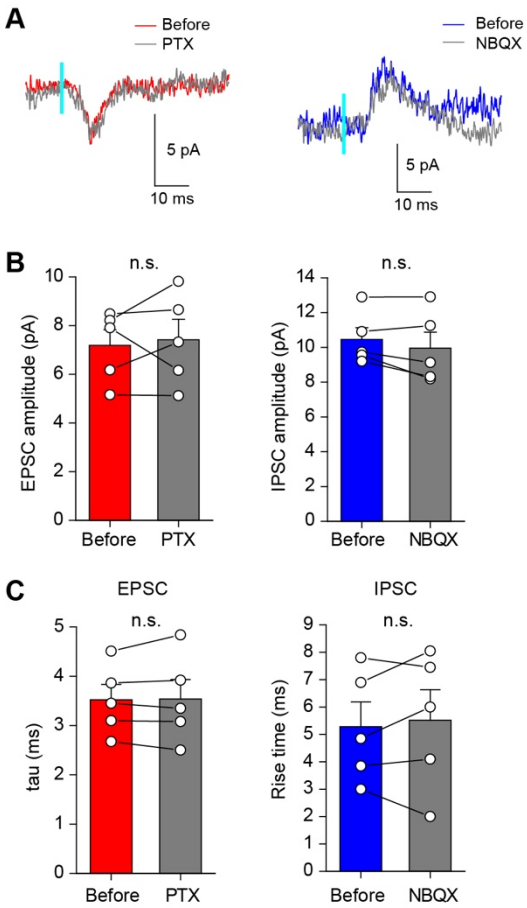

Figure 3-figure supplement 2. The amplitudes and kinetics of minimal light stimulation-evoked EPSCs or IPSCs at SuM-GC synapses were not altered by blockade of their counterpart currents

(A) Representative traces of EPSCs (left) and IPSCs (right) evoked by minimal light stimulation of SuM inputs at intermediate membrane potentials. EPSCs or IPSCs were recorded by repeating the light stimulation 100 times before, with the application of 100 μM picrotoxin (PTX) or 10 μM NBQX, respectively. **(B)** Summary plots show that the amplitudes of EPSCs and IPSCs were not changed after application of PTX or NBQX, respectively (EPSC: before: 7.2 ± 0.6 pA; PTX: 7.4 ± 0.8 pA, n = 5, p = 0.71, paired t test; IPSC: before: 10.5 ± 0.7 pA; NBQX: 10.0 ± 0.9 pA, n = 5, p = 0.18, paired t test). **(C)** Summary plots of the decay time constant of EPSCs (tau, single-exponential fit) and rise time of IPSCs (10%-90% of IPSC peak amplitude) (tau: before: 3.5 ± 0.3 ms; PTX: 3.5 ± 0.4 ms, n = 5, p = 0.84, paired t test; rise time: before: 5.3 ± 0.9 ms; NBQX: 5.5 ± 1.1 ms, n = 5, p = 0.60, paired t test). Data are presented as mean ± SEM. n.s., not significant.

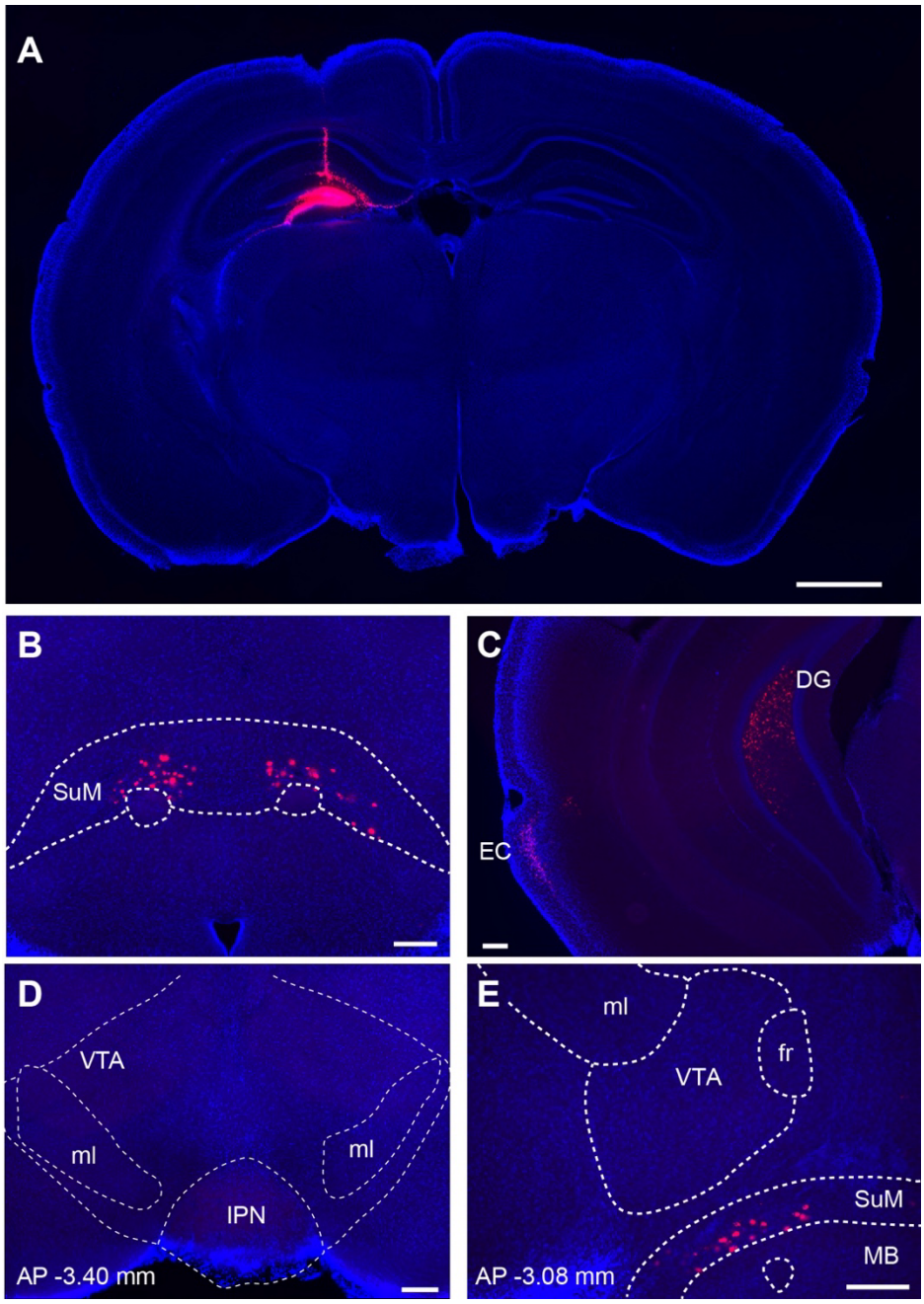

Figure 4-figure supplement 1. DG receives monosynaptic input from SuM and EC, but not from VTA.

(A) Unilateral injection of retrograde tracers (fluorescent microspheres) (red) into the dorsal DG. Fluorescence image of a coronal brain slice at the injection site. (**B**) Retrogradely labeled neurons were observed in the ipsilateral and contralateral SuM. (**C**) Ipsilateral EC cells were retrogradely labelled. **(D, E)** Retrograde labelling was not observed in the VTA at two different positions (-3.40 mm and -3.08 mm posterior to bregma) (Paxinos and Franklin, 2001). ml, medial lemniscus; IPN, interpeduncular nucleus; fr, fasciculus retroflexus; MB, mammillary bodies. Scale bars: A, 1 mm; B-E, 200 μm.

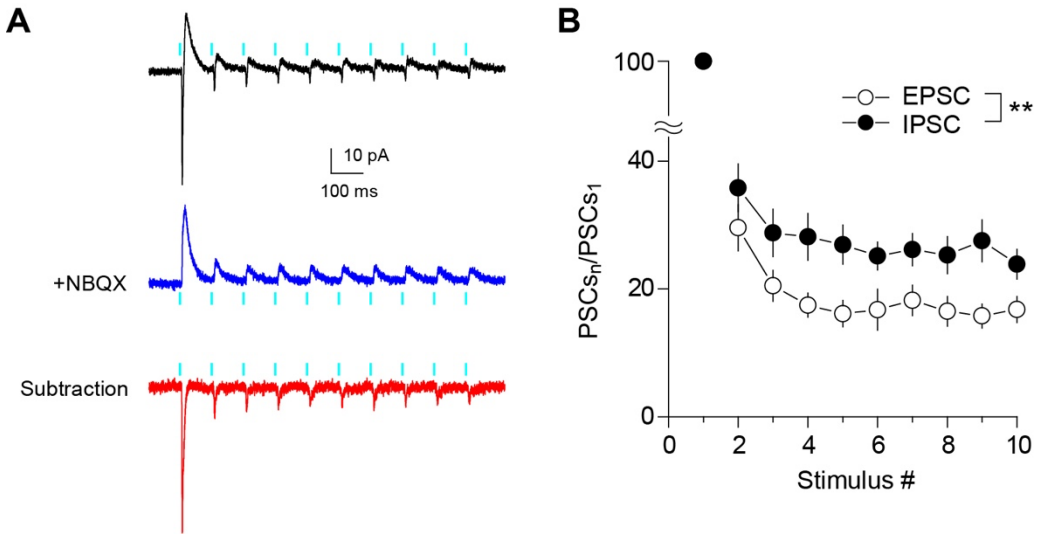

Figure 5-figure supplement 1. Short-term changes in EPSC/IPSC ratio during train stimulation at SuM-GC synapses

(**A**) Representative PSCs in response to 10 light pulses at 10 Hz recorded from GC at holding potentials of –30 mV before (black) and after application of 10 µM NBQX (blue). The EPSC (red) was isolated by subtracting the blue trace from the black trace. 1 µM TTX, 500 µM 4-AP, 50 µM D-AP5, 100 µM LY341495, and 3 µM CGP55845 were included in the extracellular solution throughout the experiments. (**B**) Summary graph of normalized EPSC and IPSC amplitudes plotted against stimulus number. Two-way repeated measures ANOVA, $F_{(1,7)} = 17.5$, $p < 0.01$, $n = 8$. Data are presented as mean ± SEM. $^{**}p < 0.01$.

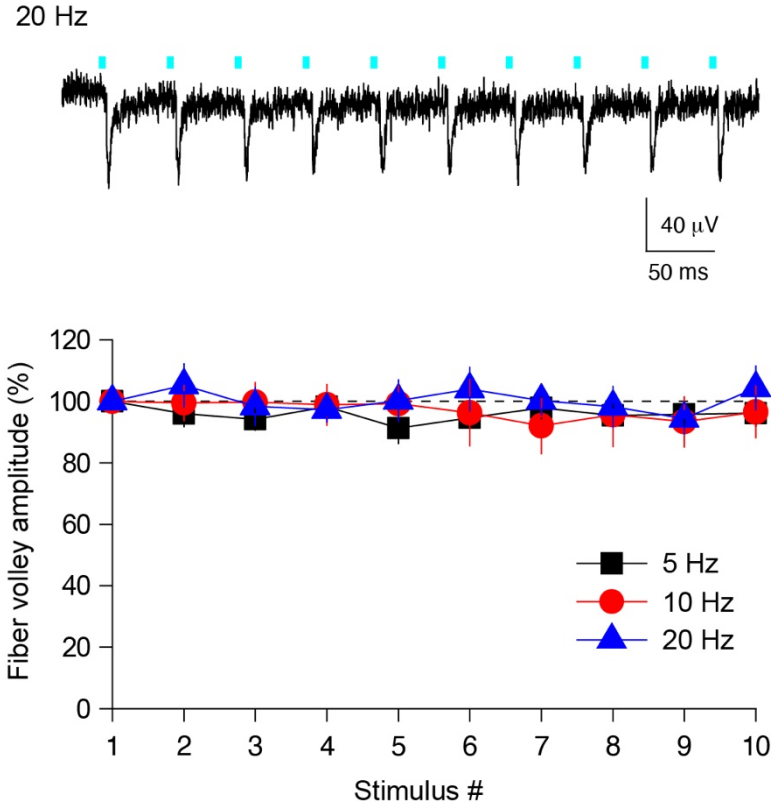

Figure 5-figure supplement 2. High fidelity activation of ChR2-expressing SuM fibers during trains

(top) Representative trace of the extracellularly recorded fiber volley from supragranular layer in response to 10 light stimuli at 20 Hz. (bottom) Summary graph of normalized fiber volley amplitude plotted against the stimulus number. 5 Hz: One-way ANOVA, $F_{(9,40)} = 0.41$, $p = 0.92$, $n = 5$. 10 Hz: One-way ANOVA, $F_{(9,50)} = 0.14$, $p = 0.99$, $n = 6$. 20 Hz: One-way ANOVA, $F_{(9,50)} = 0.35$, $p = 0.95$, $n = 6$. Data are presented as mean ± SEM.

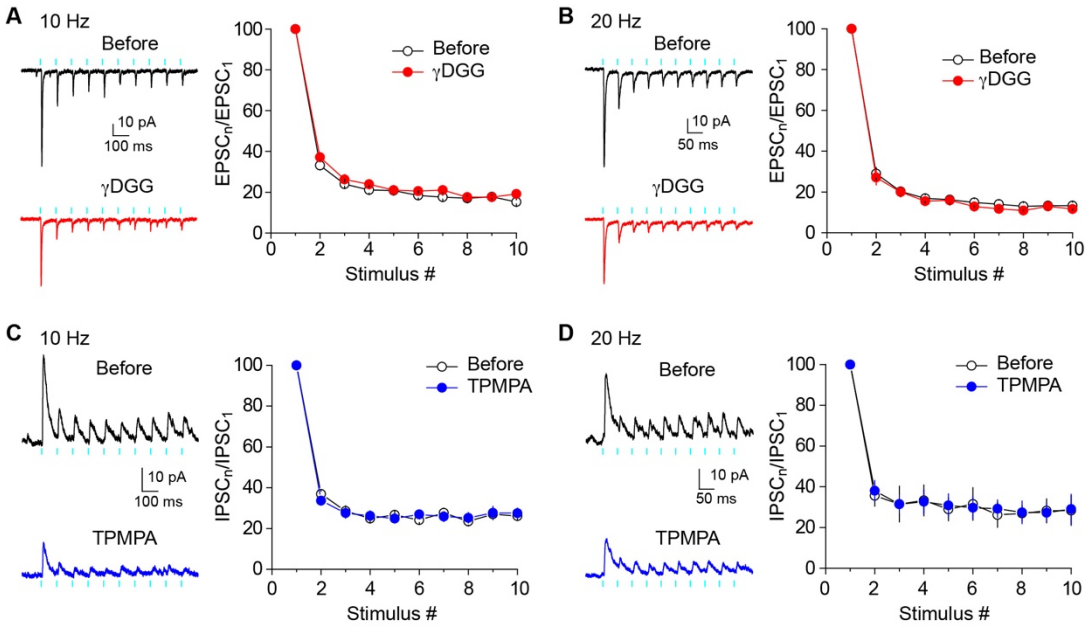

Figure 5-figure supplement 3. Preventing postsynaptic saturation and desensitization does not alter short-term depression of EPSCs and IPSCs

(**A and B**) (left) Representative traces showing EPSCs in response to 10 Hz (A) or 20 Hz (B) light stimulation before (top) and after (bottom) application of 2 mM γDGG. (right) Summary graph of normalized EPSC amplitudes plotted against stimulus number. 10 Hz: Two-way repeated measures ANOVA, $F_{(1,7)} = 1.78$, $p = 0.22$, $n = 8$. 20 Hz: Two-way repeated measures ANOVA, $F_{(1,7)} = 0.65$, $p = 0.45$, $n = 8$. (**C and D**) (left) Representative traces showing IPSCs in response to 10 Hz (C) or 20 Hz (D) light stimulation before (top) and after (bottom) application of 300 μM TPMPA. (right) Summary graph of normalized IPSC amplitudes plotted against stimulus number. 10 Hz: Two-way repeated measures ANOVA, $F_{(1,5)} = 1.02$, $p = 0.44$, $n = 6$. 20 Hz: Two-way repeated measures ANOVA, $F_{(1,4)} = 0.21$, $p = 0.67$, $n = 5$. Data are presented as mean ± SEM.

1563 **Table S1. List of primary antibodies used in the present study.**

1564

Molecules	Sequence (NCBI #)	Host	RRID	Specificity	Source	Figure
$GABA_A\alpha1$		Gp	AB_2571572	IB	(Ichikawa et al., 2011)	Fig. 4
GluN1		Ms	AB_2571605		Millipore (MAB363)	Fig. 4
VGluT2	559–582 aa (BC038375)	Gp	AB_2571621	IB	(Miyazaki et al., 2003) (MSFR106280)	Fig. 4
		Go	AB_2571620	IB	(Kawamura et al., 2006) (MSFR106270)	Fig. 4
		Rb	AB_2571619	IB	(Miyazaki et al., 2003) (MSFR106300)	Fig. 1
VGAT/VIAAT	31–112 aa (BC052020)	Rb	AB_2571622	IB	(Miura et al., 2006) (MSFR106120)	Fig. 4
		Gp	AB_2571624	IB	(Miura et al., 2006) (MSFR106150)	Fig. 1, 4
GFP		Go	AB_305643		Abcam (ab6673)	Fig. 1
		Rb	AB_2491093		(Takasaki et al., 2010)	Fig. 4

1565

1566

1567

1568

1569

1570

1571